3

Single-Molecule Imaging in Live Cells

Jie Xiao

Abstract This chapter provides a comprehensive overview of how single-molecule imaging is achieved in live cells. The main focus is on fluorescent proteins, which are the most widely used fluorescent labels for live-cell imaging. The chromophore structures and the associated photochemical and photophysical properties of fluorescent proteins are discussed in detail, with a particular focus on how they influence single-molecule imaging in live cells. A few fluorescent proteins in the yellow-to-red spectral range, including newly discovered photoinducible ones, are selected for more detailed discussions due to their superior properties in single-molecule imaging. Special considerations for live-cell imaging and general instrumentations for single-molecule detection are also described. Finally, a few representative applications using single-molecule imaging in live cells are provided to illustrate how important biological knowledge can be obtained using this powerful technique.

3.1. Introduction

Nearly 20 years ago, when the first single molecule was detected in solid at extreme temperatures [1,2], it was hard to foresee imaging a single molecule in the noisy background of a live cell. Yet now, due to the efforts of many research groups and technical advances in modern microscopes, optics, and detectors, single-molecule imaging[1] in live cells is no longer impossible.

Why is it important to image single molecule inside live cells? The reasons are multifold. First, many biologically important molecules such as transcription factors exist at low copy numbers [11,12]. In yeast, nearly 40% of genes are expressed at such low levels that their gene products are not detectable using standard fluorescence microscopy or quantitative Western blotting [11]. A more sensitive detection method—preferably at the single-molecule level—would reveal what is otherwise imperceptible. Second, due to the finite-number effect,

J. Xiao • Johns Hopkins University School of Medicine, 708 WBSB, Baltimore, MD 21205, USA

[1] Here and throughout, single-molecule imaging refers to single-fluorophore imaging. Alternatively, a single molecule can be imaged by labeling a single molecule using multiple fluorophores or detected by amplifying the fluorescent signal using a fluorogenic substrate [3–10]. These approaches are discussed briefly at the end of the chapter.

P. Hinterdorfer, A. van Oijen (eds.), *Handbook of Single-Molecule Biophysics*,
DOI 10.1007/978-0-387-76497-9_3,

the interactions of molecules at low copy numbers are often stochastic [13]. This stochasticity has been proven to contribute to molecular noise in various cellular processes such as gene expression [14–16], signal transduction [17–20], and cell fate decisions [21–25]. However, this stochasticity is often masked in ensemble measurements. Single-molecule experiments avoid ensemble averaging and allow the stochasticity of molecular interactions to be observed, providing unprecedented details about the origins and roles of molecular noise. Third, all cells (including bacterial cells) exhibit considerable heterogeneity in their cellular environments. Depending on where and when a molecule is present in the cell, its behavior may change accordingly. Single-molecule imaging allows the heterogeneity of molecular behaviors to be probed in time and space, directly correlating them with cellular states. Finally, *in vitro* single-molecule studies have contributed significantly to the understanding of how individual molecules and macromachineries work. Taking these experiments into live cells allows the direct observation of the actions of these molecules and molecular machines in a native cellular context, establishing significant physiological relevance.

It is necessary to note that this chapter focuses on the formation of an image of a single molecule in live cells on an array detector such as a charge-coupled device (CCD) rather than the collection of a signal originating from a single molecule on a point detector such as a photo avalanche diode (PAD). In this sense, single-molecule detection in live cells by fluorescence correlation spectroscopy (FCS) [26–28] and by enzymatic amplification of a fluorescent signal [9, 10] are not included, and readers are referred to the original articles and Chapter 8 for further discussion. The main focus of this chapter is to elucidate how single-molecule imaging in live cells is achieved—which fluorescent label is best suited for this purpose, what special considerations are needed, and so on—and how it can be employed to address significant biological problems. Readers are assumed to have basic knowledge of fluorescence microscopy and, wherever as needed, are referred to available literature for further discussion.

3.2. Fluorescent Labels

To probe the dynamics of biomolecules in live cells using fluorescence microscopy, the molecules have to be labeled specifically using a fluorescent probe. There are three types of labels: small organic dyes, fluorescent semiconductor quantum dots (QDs), and fluorescent proteins (FPs) (Table 3.1).

Small organic dyes need to be conjugated to purified biomolecules through *in vitro* chemical reactions and reintroduced into cells by microinjection [29]. Cell

Table 3.1. A comparison of the three commonly used fluorescent labeling schemes

	Size (nm)	Labeling	Delivery	Brightness	Photostability
Organic dyes	<1	*In vitro* chemical reaction, peptide targeting	Perfusion, microinjection	High	High
Quantum dots	10–30	*In vitro* chemical reaction, streptavidin/antibody conjugation	Endocytosis, microinjection	Extremely high	Extremely high
Fluorescent proteins	3	Genetic fusion	Endogenous	Low to high	Low to high

membrane–permeable small organic dyes can also be incubated with cells expressing the protein of interest genetically fused with a short peptide sequence that binds the dye specifically [30]. Cells are then washed to remove excess dye molecules before imaging. One advantage of using small organic dyes is that because of their small size (<1 nm), they rarely perturb the functionality of labeled biomolecules. Some organic dyes are also brighter and more photostable than FPs, and their emission spectra are far red–shifted compared to that of currently available FPs, facilitating single-molecule imaging in live cells. Indeed, organic dyes such as Cy3 [31], Cy5 [32], BodipyTR [33], and Atto647 [34] have been employed in live-cell imaging at the single-molecule level to probe receptor and membrane dynamics on the cell surface. New ones, such as the photoactivatable azido-DCDHF [35,36], are also emerging. However, this type of labeling often encounters a large fluorescence background due to the incomplete removal of excess dye molecules in the labeling reaction and nonspecific binding of dye molecules to other cellular components. For these reasons, small organic dyes are not widely used in single-molecule imaging in live cells.

Quantum dots are inorganic nanocrystals that emit strong fluorescence between 400 and 1,350 nm, depending on their sizes and chemical compositions [37]. QDs have broad and overlapping absorbance bands but narrow emission bands; therefore, one single-wavelength excitation, for example, at 488 nm, of QDs of different sizes will lead to distinct and spectrally separable emission in the visible range. QDs are often coated with streptavidin or antibodies to allow their conjugation with specific cellular target or macromolecules. The fluorescence intensities of QDs are 10- to 100-fold stronger than those of FPs and small organic dyes, and they are extremely photostable, permitting long-time tracking of tagged molecules. However, the large size of QDs (10–30 nm) precludes them from passing through cell membranes. Delivery to the inside of eukaryotic cells is often by microinjection or peptide- mediated endocytosis [38]; there is no study reporting the delivery of QDs to bacterial cells due to the presence of the cell wall.

Because small organic dyes and QDs have to be delivered into the cell through invasive methods, they are most commonly used to label proteins or lipids on the outer surface of the cell membrane. In contrast, the genetically encoded FPs are the most popular fluorescent labels for specifically labeling of molecules inside live cells. Although the size of FPs (3 nm) is larger than that of small organic dyes, and the fluorescence intensity and photostability of FPs are less impressive than those of QDs, they can be genetically engineered through molecular biological means and do not require the introduction of any exogenous cofactors to become fluorescent. The labeling of a protein by a FP is extremely specific, and the expression level of a FP fusion protein can be tuned to allow single-FP molecule detection. Because of these reasons, this chapter focuses on using FPs as the fluorescent label for single-molecule imaging in live cells. The structural, biochemical, and especially photochemical and photophysical properties (whenever available) of a collection of FPs are examined in detail, and their suitability for single-molecule imaging is discussed. The emphasis is on the underlying biophysics of FPs, knowledge of which is the prerequisite for the appropriate selection of a FP for a particular experimental design, optimization of imaging conditions, correct interpretation of single-molecule experimental data, and successful extraction of biological information from single-molecule images. A brief introduction to the discovery and structure of the *Aequorea victoria* green fluorescent protein (GFP) is first given, followed by general discussions of important spectral, photophysical, and biochemical properties of FPs, and, finally of a collection of FPs that have potential for or have been demonstrated in single-molecule, live-cell imaging.

3.3. Green Fluorescent Protein

3.3.1. Discovery of GFP

The green fluorescence of the light organs of the jellyfish *Aequorea victoria* was first described by Davenport and Nicol in 1955 [39], but the discovery of GFP, which is responsible for the green fluorescence, did not come until the early 1960s, when Osamu Shimomura and his coworkers purified a Ca^{2+}-dependent bioluminescent protein, aequorin, from luminous jellyfish at the Friday Harbor Laboratories, University of Washington [40]. They found that another protein, which was not luminescent but exhibited "a very bright, greenish fluorescence in the ultraviolet of a Mineralite," coexisted with aequorin during the early stages of the purification. They called this protein "green protein," and it was renamed "green fluorescent protein" a few years later by Hastings and Morin [41,42]. Hastings and Morin also suggested that the natural green glow of jellyfish came from the green fluorescence of GFP that was the result of the energy transferred from the aequorin protein: When aequorin binds to Ca^{2+}, it emits blue light (peaks at 469 nm) through the oxidation of its prosthetic group coelenterazine. The emitted photons are then absorbed by GFP, leading to its emission of green light (peaks at 508 nm). This was further confirmed by characterizing the photochemical properties of purified GFP [43]. The structure of the GFP fluorophore was successfully deduced by Shimomura to be a 4-(*p*-hydroxybenzylidene)-5-imidazolinone.

In the following period of more than 10 years, however, the study of GFP seemed to be at halt, possibly partially due to difficulties involved in collecting huge amount of jellyfish for purification; 100,000 jellyfish yield only less than 1/2 g of pure GFP after months of purification [43], and overhunting gradually depleted the jellyfish population in and around Friday Harbor [44]. Finally, in 1992 a critical breakthrough came as Prasher and his coworkers cloned the gene coding for GFP [45]. The expression and subsequent imaging of recombinant GFP in both *Escherichia coli* and *Caenorhabditis elegans* soon followed [46–48]. These studies revealed the most remarkable property of GFP, which is that it does not require any exogenous cofactor or enzyme except molecular oxygen to become fluorescent, and all the information for the formation of the fluorophore is genetically encoded. Thus it can be expressed and become fluorescent in foreign organisms other than jellyfish. This significantly boosted the use of GFP as a genetically encoded marker for various live-cell applications. Further development of GFP and finding of its homologs in the following years resulted in variants with fluorescence emission profiles spanning almost the entire visible light spectrum, including blue (BFP), cyan (CFP), green (GFP), yellow (YFP), orange (OFP), and red regions (RFP),[2] essentially revolutionized modern cell biology.

3.3.2. Structure of GFP and the Fluorophore

The crystal structures of jellyfish GFP (referred to as *Aequorea victoria* GFP [avGFP] from now on) and an enhanced GFP mutant [49] (S65T, [EGFP]) were solved independently by two groups in 1996 [50,51]. Both GFPs adopt a cylindrical fold of 11-stranded β-barrels wrapped around a single central helix, with a diameter about 30 Å and a length of about 40 Å (Figure 3.1A). The fluorophore is located on the central helix, almost at the geometric center of the cylinder. The top and bottom of the barrel are capped by small, somewhat distorted

[2] In the field of fluorescent proteins, the wavelength of each color is defined slightly differently from what is defined in physics. Following the convention of the field, in this chapter the wavelength of each color is as follows: violet: ~400 nm; blue: ~480 nm; green: ~510 nm; yellow: ~550 nm; orange: ~580 nm; red: ~620 nm.

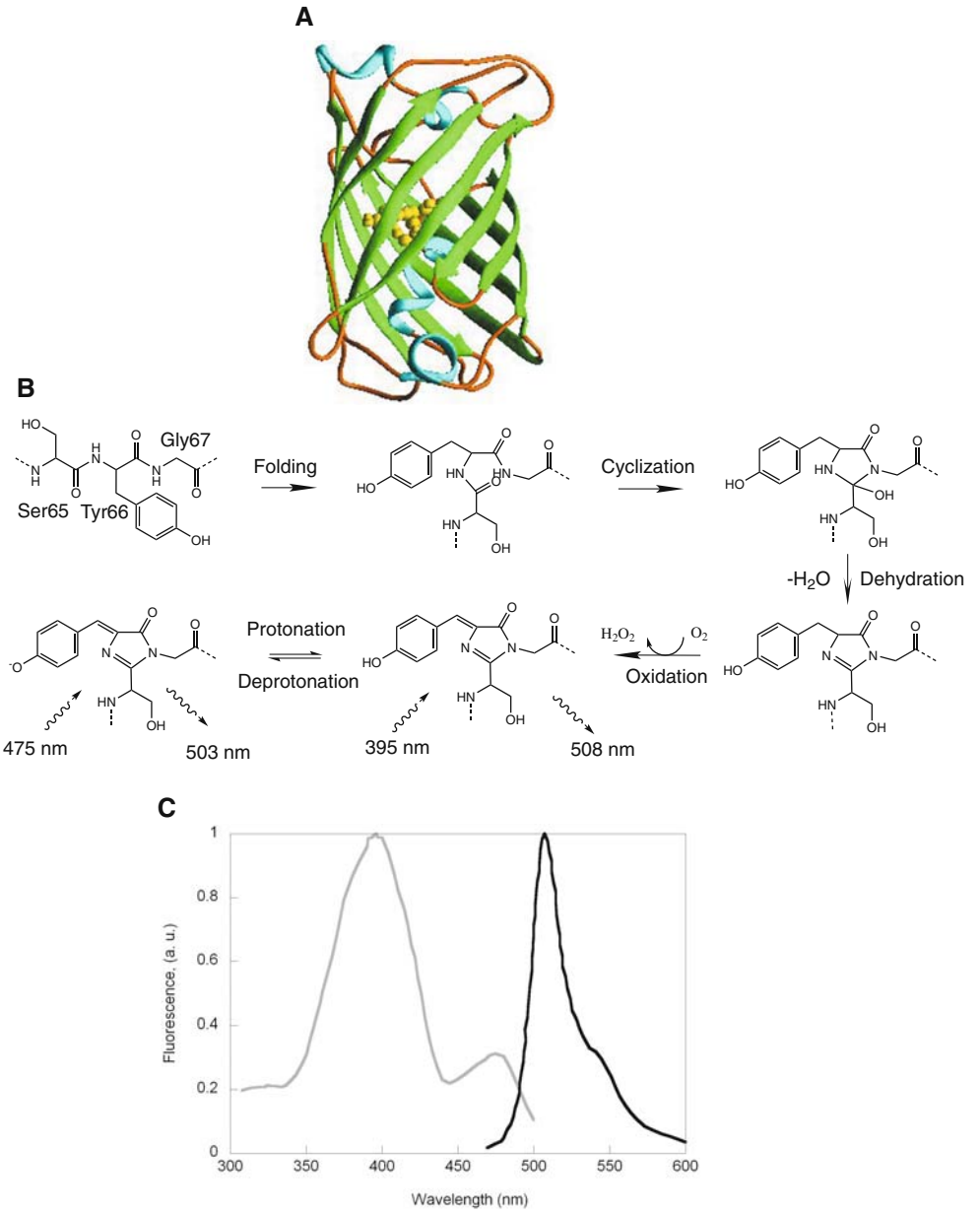

Figure 3.1. Crystal structure of green-fluorescent protein (GFP) from *Aequorea victoria* (**A**) [50], the fluorophore maturation process (**B**), and its excitation (*gray*) and emission (*black*) spectra (**C**).

sections of α-helix. The hydrogen bonds formed by the tightly fitted β-sheet strands and the caps at the top and bottom of the barrel serve well for the extraordinary stability of GFP, and at the same time shield the fluorophore from quenching by colliding water or oxygen molecules. All available FPs, natural or engineered, share the same cylindrical fold, although there may be extensive differences in the primary sequences.

The fluorophore of avGFP is formed by the posttranslational, covalent modifications of three amino acids, Ser65, Tyr66, and Gly67, which only occurs after the protein folds into its native state [47,52–56]. The fluorophore forms an extensive hydrogen-bonding network with surrounding residues, and the state of bonding changes the spectral and photophysical properties of the fluorophore substantially. The following describes the accepted mechanism of fluorophore formation, although some mechanistic details are under debate [55–57] (Figure 3.1B). The first step is the cyclization of the tripeptide main chain by the nucleophilic attack of the amide nitrogen of Gly67 at the carbonyl carbon of Ser65, generating a heterocyclic intermediate. The second step is the dehydration of the five-member heterocyclic ring, which leads to the formation of an imidazolinone ring. The oxidation of this intermediate by molecular oxygen at the position of Tyr66 C_α–C_β then finally produces a full π conjugation that extends from the phenolic group of Tyr66 to the imidazolinone ring in *cis* configuration—the mature GFP fluorophore. Among these steps, the final oxidation by molecular oxygen is rate limiting, with a time constant of about 2 hr for avGFP [53].

The absorption spectrum of avGFP has two peaks—a major one at 395 nm and a minor one at 475 nm (Figure 3.1C). Excitation at 395 and 475 nm gives similar but not identical emission spectra peaking at 508 or 503 nm, respectively [47]. Based on pH-dependent studies, it was shown that the 395-nm absorption peak is due to the protonated phenol (Tyr66) in the fluorophore, whereas the 475-nm peak is due to the deprotonated form [47,58]. Of interest, the former undergoes excited-state proton transfer (ESPT), as the neutral fluorophore becomes more acidic in the excited state [59], to become the anionic fluorophore, giving a similar but not identical emission peak at 508 nm [60,61].

In all naturally occurring GFP-like proteins (>100), four amino acids—two in the fluorophore tripeptide, Tyr66[3] and Gly67, and two that directly interact with the fluorophore through hydrogen bonding, Arg96 and Glu222 (avGFP numbering)—are absolutely conserved [64]. This suggests that the basic mechanisms of fluorophore formation in different GFP-like proteins are similar. Indeed, so far all mature fluorophores of available FPs share one common feature, which is the oxidized tyrosine C_α–C_β bond. However, the subsequent modifications of the GFP fluorophore, which change the extension of the π systems, either by natural evolution or human-made engineering, produce various FPs with colors extending from blue to far red.

3.4. Properties of Fluorescent Proteins

This section will discuss important spectral, photophysical, and biochemical properties of FPs. The goal is to equip the reader with a clear understanding of these important parameters so that when it comes to choosing which FP to use in a particular experiment, the researcher will know which property of different FPs to compare.

3.4.1. Brightness

The most essential parameter to ensure successful single-molecule imaging is the brightness of the fluorophore. At the ensemble level, brightness (B_e) is defined as the product

[3] It is unclear why Tyr66 is universally conserved in all GFP-like proteins in nature. In engineered FPs it was found that other two aromatic groups, Trp and Phe, or even His, can substitute Tyr66 and produce blue-shifted fluorescence as in CFPs and BFPs [47,62,63].

of molar absorption coefficient (ε, M^{-1} cm^{-1}) and quantum yield (Φ) at a particular pair of excitation and emission wavelengths:

$$B_e = \Phi_{\lambda ex/\lambda em} \cdot \varepsilon_{\lambda ex}$$

At the single-molecule level, the brightness is defined as

$$B_s = \Phi_{\lambda ex/\lambda em} \cdot \sigma_{\lambda ex} = \Phi_{\lambda ex/\lambda em} \cdot \frac{2.303\varepsilon_{\lambda ex}}{N_A}$$

where $\sigma_{\lambda ex}$ is the absorption cross section of a single molecule in cm^2, which can be calculated from ε using the Avogadro number, N_A.

In a typical experiment, the number of photons emitted by a single fluorophore during a particular exposure time can be calculated from its photon emission rate, which is related to its brightness, in that

$$I_{\lambda em} = I_{\lambda ex} \cdot B_s$$

where $I_{\lambda em}$ is the photon emission rate in photons per second per molecule and $I_{\lambda ex}$ is the incident light intensity in photons per second per square centimeter. For example, given an incident light flux of 514 nm at 200 W/cm^2, a typical room-temperature fluorophore absorption cross section at 2 $Å^2$, and a quantum yield of 0.6, the photon emission rate can be calculated to be $\sim 6 \times 10^4$ photons/sec. If an exposure time of 100 ms is used and the overall microscope detection efficiency is 5%, then ~300 photons will be detected during the 100 ms. This amount of photons is more than enough to enable single-molecule imaging; many detectors are capable of single-photon detection. However, the available photons become a major limitation when a reaction time course is monitored and the total photons are spread over a number of separate frames. In addition, as discussed later, a high brightness is necessary but not sufficient to achieve single-molecule detection in live cells because the photobleaching property of the fluorophore and the autofluorescence background of live cells complicate detection. In practice, an experience-based empirical threshold of brightness can be set at about a B_e of 3×10^4 (B_s of 1.0) to ensure that a single fluorophore will emit enough photons to allow its detection at the single-molecule level. Depending on the emission wavelength, this threshold for selecting fluorophores will change. For example, in the blue/green region a fluorophore that is brighter than the empirical threshold is usually needed because cells' autofluorescence background is higher at these wavelengths, whereas in the red region the threshold could be lower because the autofluorescence background is lower.

3.4.2. Fluorescence Lifetime

Fluorescence lifetime is another important parameter of a fluorophore. It measures on average how fast a fluorophore emits a photon, thus determining the saturating excitation intensity required to extract all possible photons in the shortest time. However, in live-cell imaging this scenario is rarely if ever encountered. Besides this, most FPs suitable for live-cell imaging have similar fluorescence lifetimes in the range of a few nanoseconds, rendering gating fluorescence lifetime difficult. Therefore, this parameter usually has little influence when choosing an appropriate FP.

3.4.3. Photobleaching Quantum Yield

Photobleaching is the process of irreversible destruction of a fluorophore in its excited state due to its interactions with molecular oxygen or other surrounding molecules. The fluorophore may be chemically modified and return to the ground state as a new molecule that no longer absorbs light at the excitation wavelength, For example, it was reported that photobleached enhanced yellow-fluorescent protein (EYFP) molecules irreversibly lose a mass of 44 daltons, possibly due to the decarboxylation of the E222 residue during intense laser illumination [61,65]. The exact photobleaching mechanisms of FPs in live cells have not been elucidated, and different FPs may have different mechanisms due to different structural flexibility and local fluorophore environments. For example, photobleaching of mOrange and TagRFP-T are reported to be sensitive to the presence of oxygen [66], while EGFP is insensitive to oxygen, singlet oxygen, or general radicals [67–69]. It has also been reported that when a FP molecule bleaches, it emits one singlet oxygen, which could further damage adjacent FP molecules [70,71].

Quantitatively, the sensitivity of a fluorophore to photobleaching is described by its photobleaching quantum yield Φ_b, defined as the probability of photobleaching per photon absorbed, that is, the reciprocal of the average number of excitation/emission cycles a fluorophore can undergo before it photobleaches. When multiplied by the quantum yield, the product represents the average number of photons a fluorophore can emit. For organic dyes used in single-molecule studies, Φ_b is usually in the range around 10^{-6}, while that for FPs is around 10^{-5} [68,72–74].

Photobleaching quantum yield is also a key parameter in determining whether the fluorophore is suitable for single-molecule imaging because it limits how many photons can be collected before a fluorophore is irreversibly destroyed. For example, if a fluorophore is dim but highly photostable (low Φ_b), one may compromise time resolution to accumulate enough photons using long integration time. However, if a fluorophore is photoliable (high Φ_b), it may only emit a few photons before it photobleaches, rendering its detection difficult even if it has a high brightness.

Φ_b is dependent on the particular molecular structure of a fluorophore and its local environment but not on excitation intensity or how excitation is delivered (continuous or pulsed). Therefore, Φ_b can be used to compare the photostability of fluorophores across different spectral classes and in different experimental setups. By definition, Φ_b is best measured at the single-molecule level, where the number of photons each fluorophore emits before it photobleaches is counted and the average Φ_b calculated. Note here that although the total number of photons a fluorophore can emit before it photobleaches is independent of excitation intensity, the photon emission rate of the fluorophore is. The stronger the excitation intensity, the higher is the photon emission rate, and thus the shorter is the time the fluorophore will fluoresce. If achieving longer time traces is the goal, low excitation intensity should be used at the sacrifice of lower signal levels per acquisition time.

Currently published photostability measurement of FPs were usually done at the ensemble level by monitoring the time at which the photon emission rate of high-concentration fluorophores has dropped to half of its initial rate under arc lamp illumination [75]. This method does not allow the calculation of the absolute Φ_b values but still provides a qualitative comparison among different FPs that are measured under the same experimental conditions. However, the time constants in this type of ensemble measurements are often much longer than what would be obtained in single-molecule measurements [76]. This is likely due to the fact that in the ensemble there are molecules existing in dark states that do not

fluoresce immediately at the onset of excitation [68], whereas in single-molecule experiments the true photobleaching time can be obtained by recording only the time when a fluorophore is fluorescent. In addition, the ensemble photobleaching time curves often exhibit multiphasic exponential decay, which cannot be simply described by one time constant. Because of these considerations, a systematic characterization of the photobleaching quantum yields of available fluorophores at the single-molecule level is much needed.

In most single-molecule experiments (especially tracking experiments), photostability of a fluorophore is preferred to obtain long trajectories. However, photobleaching can also be used to one's advantage. For example, in gene expression experiments in which accumulation of fluorescent background by newly expressed FP molecules is a problem, a photolabile FP such as the YFP variant Venus is preferred so that the previously generated molecules can be quickly photobleached to allow the next round of detection.

3.4.4. Fluorescence Blinking

Fluorescence blinking is the switching of a fluorophore between a fluorescent and a nonfluorescent state spontaneously on a time scale usually ranging from milliseconds to seconds. At the ensemble level, blinking of individual molecules is not observed, and this behavior merely reduces the average fluorescence intensity because the on- and off-switching of individual molecules is stochastic and averaged out in large ensembles. At the single-molecule level, however, it is important to take the blinking behaviors of individual molecules into account to avoid misinterpretation of data.

Nearly all fluorophores exhibit some kinds of dynamic blinking behaviors on different time scales. In live-cell imaging, the integration time is usually in the range of a few to a few hundreds of milliseconds. Therefore, only blinking at that time scale is considered in the following text because faster or slower blinking behaviors will not be reflected in the measurements.

The on-off blinking behavior was first reported on EGFP [69] and YFP [77]. Figure 3.2 shows one typical time trace of a single YFP (Venus) molecule on continuous illumination at 514 nm. It is evident that the fluorescence intensity fluctuates between bright (on) and dark (off) states on the time scale of seconds. A three-level system has been proposed to explain the blinking behavior. The on-state is the result of photon emission during the transitions from the singlet excited state to the ground state, as described in a standard fluorescence two-level system. During this cycle, however, there is a small probability that a molecule will go into a long-lived dark state that cannot emit a photon. This contributes to the off-period. Only when the molecule is returned to the singlet ground state capable of absorbing new photons will fluorescence resume. The transition probability from a bright to dark state can be calculated by taking the reciprocal of the average number of excitation/emission cycles during the on-time, which has been measured to be at about 5×10^6 for enhanced GFP (EGFP) [74]. The average off-time for both EGFP and EYFP was measured to be between a few and a few tens of seconds [65,68,74,77].

The exact nature of the molecule at the dark state, however, has not been completely elucidated. It was first proposed that the protonated fluorophore is responsible for the off-state and that the conversion between protonation and deprotonation of the fluorophore results in the blinking behavior—the anionic form of the fluorophore fluoresces, while the protonated form does not [77]. Later this process turned out to be more complicated than expected. McAnaney et al. demonstrated that at sufficiently low power densities (<1 kW/cm^2), the ground-state protonation and deprotonation is indeed responsible for the blinking behavior

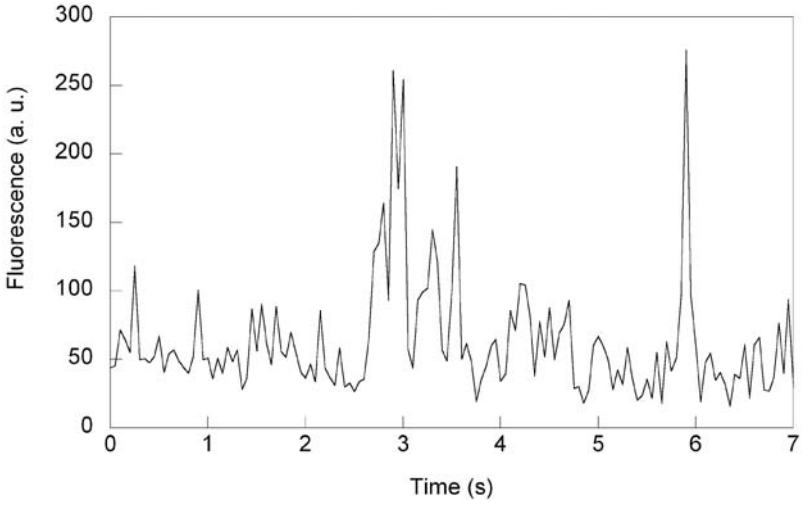

Figure 3.2. Fluctuations (blinking) in the fluorescence intensity of a single yellow-fluorescent protein (YFP) Venus molecule under continuous illumination of 514 nm at 2 kW/cm^2 with an integration time of 50 ms.

[65]. However, Peterman et al. showed that there is a clear excitation power dependence—between 0.5 and 5 kW/cm^2 the fluorescence on-time becomes shorter when the power gets higher. In addition, at high excitation intensity (5 kW/cm^2), the average fluorescence on-time is independent of pH between 6 and 10 [68]. These experiments suggest that at high power densities, the photon-driven excited-state protonation reaction of the fluorophore is faster than the ground-state process [65,74,78]. The fluorescence off-time, however, was found to be independent of excitation power [68], indicating that YFP molecules in the off-state spontaneously relax to the on-state [65,79]. Moreover, photon-induced isomerization of the fluorophore conformation [80] and rearrangement of hydrogen-bonding network around the fluorophore [81] have been suggested to contribute to the blinking behavior.

3.4.5. Maturation Time

The fluorophore maturation process in FPs determines how fast a fluorescent response can be detected following the production of a FP molecule. The oxidation step of the fluorophore formation process as described earlier is usually the slowest and is thus considered the rate-limiting step for the maturation process. To speed up the maturation process, increased access of the fluorophore to molecular oxygen is important [82]. However, it is possible that this increased accessibility may also lead to increased environmental sensitivity and proneness to photobleaching. For some cellular processes that do not require the detection of a FP molecule immediately after its production, slow maturation is of less concern. However, a cell expressing a fast-maturing FP will contain more copies of fully matured FP than a cell expressing a slow-maturing FP at the steady state, affecting data throughput of an experiment. If monitoring the fast dynamics of cellular processes such as gene expression is the goal, using a fast-maturing FP as the gene expression reporter is critical. Because gene regulation is mainly controlled by differential binding modes of transcription factors, changes of gene expression state usually occur on the time scale of a few minutes or even shorter. To follow this process faithfully with a high time resolution, a FP reporter molecule needs to become

fluorescent as soon as it is synthesized. Unfortunately, all current FPs mature slowly, on the time scale of a few tens of minutes to a few hours, except one YFP variant, Venus, which has a maturation time constant measured at about 2 min *in vitro* and 7 min *in vivo* [83,84]. This property makes Venus an attractive gene expression reporter, allowing the direct counting of protein molecules generated one at a time [84]. If another fast-maturing FP emitting in the red region were developed, the temporal expression correlation of two related genes could be monitored simultaneously at the single-molecule level, greatly facilitating the investigation of gene regulation mechanisms in large networks.

3.4.6. Construction and Expression of Fusion Proteins

It is critical that being tagged by a FP does not perturb the function of the tagged protein. Before a single-molecule experiment is conducted, one should verify whether the fusion protein is functional. This can be done in different ways. The most stringent test is to check whether the expression of the fusion protein in a cell strain that has the gene for the untagged protein deleted will rescue the deletion phenotype, provided that the deletion of the wild-type gene has an identifiable phenotype. If no obvious phenotype of the deletion strain can be identified, one should verify whether other genetic and biochemical properties of the fusion protein, such as expression level, cellular localization pattern, enzymatic activity, or gene regulation activity, reproduce those of the untagged protein. Based on empirical observations, in general GFPs cause least perturbations to the tagged proteins, while some engineered RFPs and especially some photoinducible FPs such as rsFastLime and EosFP (discussed later) are difficult to work with. In the latter cases, when the fusion protein is not functional, the linker sequence needs to be carefully scrutinized, and changing the terminus to which the FP is fused may improve the performance of the fusion protein. It was found that by fusing the first and last seven amino acid residues of avGFP to the N and C termini of some RFPs, the tolerance of the tagged proteins to the RFP fusions was enhanced [85]. In some cases, lowering the expression temperatures helped to improve the folding of the fusion proteins.

To enable single-FP-molecule detection in live cells, it is necessary to repress the expression level of the fusion FP protein to avoid large fluorescence background. In bacterial cells, this can be done by using a weak or repressed promoter such as the *lac* promoter and incorporating the gene encoding the fusion protein into chromosome or a single-copy plasmid such as the F plasmid. In eukaryotic cells, a regulated promoter such as the cytomegalovirus (CMV) promoter repressed by Tet repressors can be used. The original chromosomal gene of the tagged protein can be left intact. In the case of photoinducible proteins (see later discussion), however, the expression level does not have to be strongly repressed because high concentrations of FP can be expressed with only a few molecules becoming fluorescent upon photoinduction.

3.4.7. General Guidelines

In general, a FP suitable for single-molecule imaging in live cells should possess one or more of the following properties: high brightness, high photostability, emission in the visible range, and fast maturation time. Note that although the monomeric state of the FPs was not discussed earlier, it is mandatory for protein tagging. This is because dimeric or tetrameric FPs tend to cause self-association and aggregation of tagged proteins, preventing proper interpretation of experimental data [75]. All the FPs to be discussed are monomeric. One should also keep it in mind that there is no single FP that can meet the demanding criteria of all

experiments. Therefore, one needs to decide what the most important property for a particular experiment is and make the necessary compromise. In the following section a collection of FPs that have the potential or have already been demonstrated in single-molecule imaging in live cells is discussed in detail. Their properties are compiled in Tables 3.2 and 3.3.

3.5. Derivatives of avGFP and Other GFP-Like Proteins

Extensive mutagenesis efforts have been exerted on the original avGFP to improve its properties. This is because the avGFP has complicated photochemistry [86,87], does not fold well above room temperature [58], and matures slowly [47]. Through the combination of random mutagenesis and rational design, different versions of FPs have been generated, with their absorption and emission wavelengths blue- or red-shifted as much as 40 nm and with improvements in their fluorescence brightness, photostability, environmental sensitivity, folding, and maturation kinetics (Figure 3.3 and Table 3.2) (for extensive reviews, see Refs. 75 and 86]).

For example, the first EGFP (Figure 3.3) has an S65T mutation, which diminishes the 395-nm absorption peak of the avGFP but significantly enhances the 475-nm peak, greatly facilitating excitation in the blue region instead of the violet region, with the latter being usually detrimental to cells [47,49,88]. This is possibly because the threonine at position 65 is bulkier than the original serine and cannot adopt the same conformation as Ser65 to donate a hydrogen bond to Glu222. This change leads to changes in the hydrogen-bonding status of a few polar residues around the fluorophore, and the phenolic hydroxyl group of Tyr67 is effectively anionized, contributing to the greatly enhanced absorption at 475 nm [51,89]. Another example is the YFP class. The red-shifted excitation and emission (515 and 525 nm, respectively) of YFPs is mainly due to the T203Y mutation, where the tyrosine stacks its aromatic ring next to the phenolate anion of the fluorophore, forming an extended $\pi-\pi$ interaction and lowering the excited-state energy level (Figure 3.3) [63,90].

Among many improved versions of avGFP, the YFP class is preferable over GFPs for single-molecule imaging in live cells due to its superior spectral properties [76], the reduced cellular autofluorescence at YFP emission peaks, and the available high-quality imaging optics and detectors. Blue or cyan FPs are usually not considered for single-molecule imaging in live cells because of the presence of prominent cellular autofluorescence in their spectral region, increased phototoxicity to cells caused by ultraviolet (UV)/violet excitation, and low detection efficiency of UV optics and detectors. For the GFP class, although improved GFPs such as EGFP has been successfully applied to single-molecule imaging in live cells to reveal cell surface protein distribution patterns [91] and actin filament dynamics [92], and the newly developed superfolder GFP (sfGFP) [93] possesses the necessary brightness for its single-molecule detection, this class does not have a clear advantage over the YFP class or the RFP class in single-molecule live-cell imaging. Therefore, blue and green FPs are not included here.

3.5.1. Derivatives of avGFP

EYFP

Enhanced YFP (EYFP) contains four mutations (S65G, V68L, S72A, and T203Y) compared to avGFP. As discussed earlier, the T203Y mutation is rationally designed to shift

Table 3.2. Properties of selected fluorescent proteins that have potential or have been demonstrated in single-molecule imaging in live cells

	Ex (nm)	Em (nm)	ε (M^{-1} cm^{-1})	σ ($Å^2$)[1]	Φ	B_s[2]	Φ_{bl}[3a] ($\times 10^{-5}$)	Photostability[3b] (sec)	$\tau_{maturation}$ (min)[4]	pKa[5]	SMD[6] *in vitro*	SMD[7] *in vivo*
EGFP[8]	488	507	53,000 [214]	2	0.60 [214]	1.2	6.9 [76]	174	94 [82]	6.0	[76,215,68,69]	[91,92]
sfGFP	485	510	83,300 [93]	3.2	0.65 [93]	2.1	ND	157	ND	5.5	NP	NP
EYFP[9]	514	527	83,400 [63]	3.2	0.61 [63]	1.9	6 [76]	60	6.6 [83]	6.9 [83]	[65,68,76–78]	[33,94–96,202]
Citrine	516	529	77,000 [100]	2.9	0.76 [100]	2.2	2.6 [73]	49	ND	5.7 [100]	[73]	[216]
Venus	515	528	92,200[10] [83]	3.5	0.57 [83]	2.0	ND	15	2.0 [83]	6.0 [83]	NP	[84,196]
Ypet	517	530	104,000 [103]	4.0	0.77 [103]	3.1	ND	49	ND	5.6 [103]	NP	NP
mKO	548	559	51,600 [117]	2	0.60 [117]	1.2	ND	122	ND	5.0	NP	NP
mOrange2	549	565	58,000 [66]	2.2	0.60 [66]	1.3	ND	228 [66]	390 [66]	6.5	NP	NP
tdTomato	554	581	138,000 [85]	5.3	0.69 [85]	3.6	ND	98	87 [85]	4.7	NP	[170]
TagRFP-T	555	584	81,000 [66]	3.1	0.41 [66]	1.2	ND	337	144	4.6	NP	NP
mCherry	587	610	72,000 [85]	2.8	0.22 [85]	0.6	ND	96	22 [85]	<4.5	[218]	[116]
mKate	588	635	45,000 [122]	1.7	0.33 [122]	0.6	ND	166	108 [122]	6.0 [122]	NP	NP

[1] The cross section σ of single molecules is calculated from the ensemble molar extinction coefficient ε and expressed in $Å^2$.
[2] Brightness at the single-molecule level expressed as the product of cross section σ and quantum yield Φ, in units of $Å^2$.
[3a] Photobleaching quantum efficiency measured at the single-molecule level. For most fluorescent proteins (FPs) this parameter is not determined.
[3b] Photostability was measured at the ensemble level by the time (in seconds) it takes for the photon emitting of each FP to drop to half of its initial value at 1,000 photons/sec under continuous illumination of an arc lamp. Values of photostability are taken from Ref. 75 if not specifically indicated.
[4] Time constant of the oxidation step during the maturation of the chromophore. In some published work the maturation half-life $\tau_{1/2}$ was used. In this table published $\tau_{1/2}$ is converted to $\tau_{maturation}$ using $\tau_{maturation} = \tau_{1/2}/\ln(2)$.
[5] The values of pKa are taken from Ref. 75 if not specifically indicated.
[6] Representative published work involving single-molecule detection *in vitro*.
[7] Representative published work involving single-molecule detection *in vivo*.
[8] The commonly used enhanced green-fluorescent protein (EGFP) from Clontech is the GFPmut1 variant containing F64L and S65T mutations [88]. The listed ε (23,000 M^{-1} cm^{-1}) and Φ (0.7) from Clontech at http://www.clontech.com/upload/images/downloads/fp_overview_and_apps_CDv2.zip are lower than those listed in the table and have not been verified.
[9] Enhanced yellow-fluorescent protein (EYFP) contains S65G, V68L, S72A, and T203Y mutations and was called 10C in the original publication [63].
[10] In two other studies [103,217] the molar extinction coefficient and quantum efficiency of Venus were measured at ~105,000 and ~0.7, respectively. The differences may be due to the different percentages of nonfluorescent protein in the protein preparation.
Em, emission; ex, excitation; mKO, monomeric orange-fluorescent protein Kusabira-Orange; ND, not determined; NP, not published; sfGFP, superfolder green-fluorescent protein; YPet, yellow-fluorescent protein for energy transfer.

Table 3.3. Properties of photoinducible fluorescent proteins

	Pre-photoinduction				Photoinduction wavelength/Φ[1]	Reversibility	Post-photoinduction				pKa	Ref.	SMD *in vitro*	SMD *in vivo*
	Ex (nm)	Em (nm)	σ (Å^2)	Φ			Ex (nm)	Em (nm)	σ (Å^2)	Φ				
Dronpa	NA	NA	NA	NA	405 nm/0.37	Yes (488 nm/3.2×10^{-4})	503	518	3.6	0.85	5	[127]	[138,145,158]	NP
rsFastLime	NA	NA	NA	NA	405 nm/0.37 or none	Yes (488 nm/0.17)[2]	496	518	1.5	0.77	ND	[140]	[152]	NP
rsCherry	NA	NA	NA	NA	550 nm/ND	Yes (450 nm/ND)	572	610	ND	ND	ND	[153]	[153]	NP
rsCherryRev	NA	NA	NA	NA	450 nm/ND	Yes (550 nm/ND)	572	608	ND	ND	ND	[153]	[153]	[153]
Dendra2	490	507	1.7	0.50	405 or 488 nm/ND	No	553	573	1.3	0.55	6.6–6.9	Evrogen [131]	NP	[159]
mEosFP (tdEosFP)	505	516	2.6	0.64	405/ND	No	569	581	1.4	0.62	5.8	[130]	[158,130,150]	[123]

[1] Φ is the photoinduction quantum efficiency. In the case of rsFastlime, it is assumed to be the same as that of Dronpa because the measured switching-on rates for Dronpa and rsFastlime are similar to each other [140]. rsFastlime can also spontaneously relax to the fluorescent state without the need for an activation laser line.

[2] The switching-off quantum efficiency of rsFastlime is calculated based on the switching-off rate ratio between rsFastlime and Dronpa [140].

[3] The quantum efficiency and absorption cross section of rsCherry and rsCherryRev have not been measured, but fluorescence correlation spectroscopy study shows that at the single-molecule level they have similar brightness to mCherry [153].

Em, emission; Ex, excitation; NA, not applicable; ND, not determined; NP, not published.

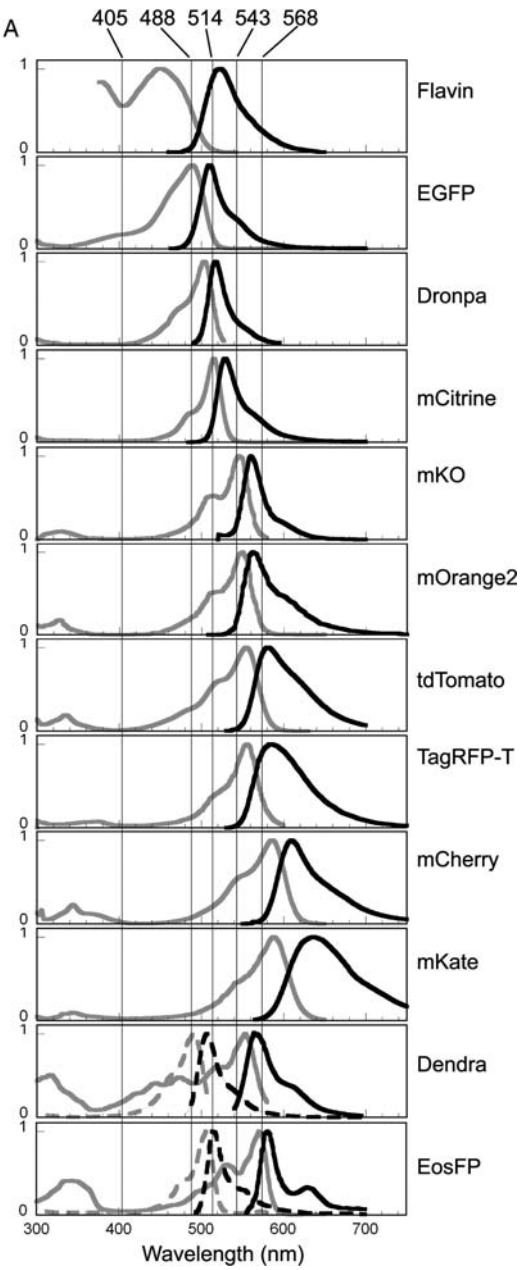

Figure 3.3. Comparison of fluorescence excitation (*gray*), emission (*black*) spectra (**A**), and the corresponding fluorophore structure of fluorescent proteins (FPs) as discussed in the text (**B**). The excitation and emission spectra of flavin adenine dinucleotide (FAD) are also shown as a comparison. For the photoconvertible FPs Dendra and EosFP, the spectra of green forms are shown in broken lines and red forms in solid lines. For each fluorophore the conjugated π system is color-coded for its emission wavelength. For the yellow-fluorescent protein (YFP) class, only mCitrine's spectra and fluorophore structure are shown because they are representative for other YFPs such as enhanced yellow-fluorescent protein (EYFP), Venus, and YFP for energy transfer (YPet). The spectra of rsFastlime, rsCherry, and rsCherry-Rev are not shown because they are similar to their corresponding parents Dronpa and mCherry with slight wavelength shift, respectively (see Table 3.3 for details). The crystal structures of fluorophores in some FPs are not

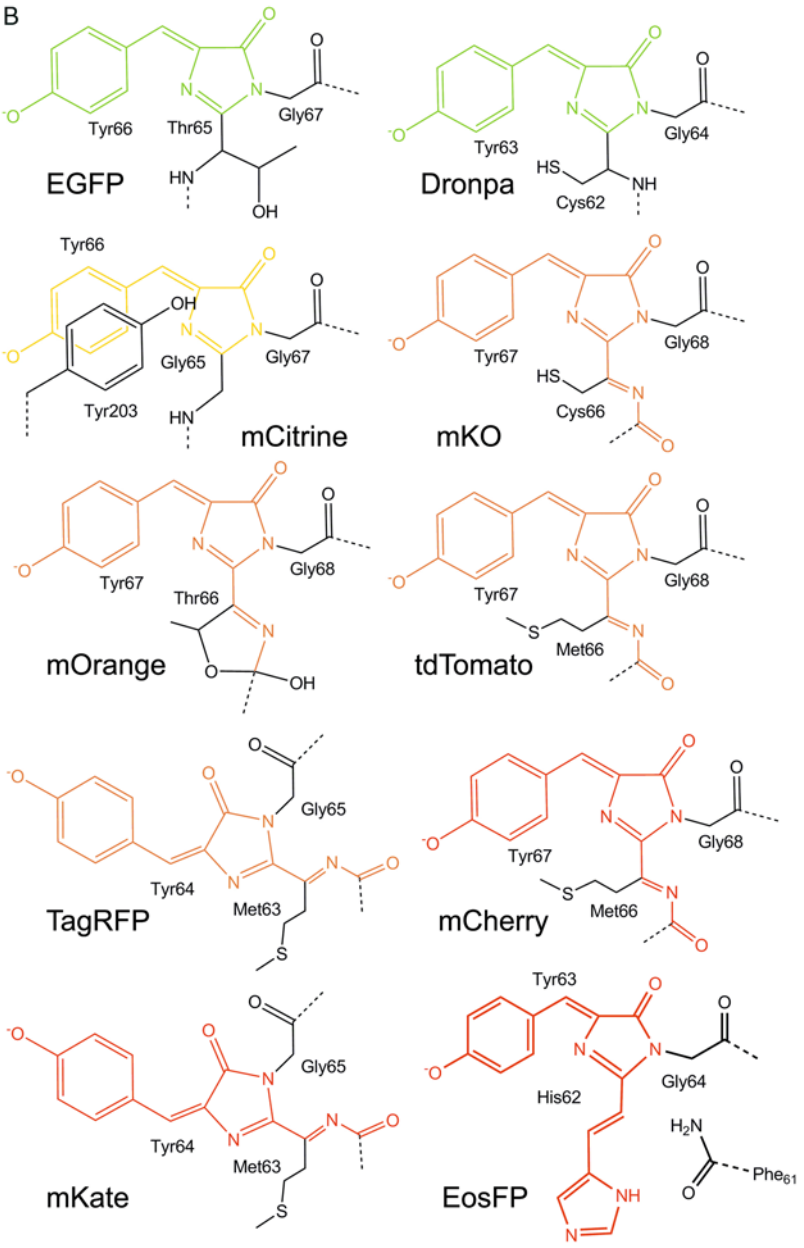

Figure 3.3. (continued) available, and the shown structures are modeled based on the closest available structures when possible: monomeric orange-fluorescent protein Kusabira-Orange (mKO) and tdTomato from *Discosoma striata* red-fluorescent protein (dsRed) [112,113], mOrange2 from mOrange [118], and TagRFP-T and mKate from eqFP611 [121]. For Dendra the mechanism for its photoconversion is unclear, and therefore its chromophore structure is not shown. Five commonly used laser lines at 405 (solid state), 488 (argon ion), 514 (argon ion), 543 (helium neon), and 568 nm (krypton) are superimposed on the spectra to indicate which laser line is best suited for the excitation of which FP. EGFP, enhanced green-fluorescent protein.

emission into the yellow-green region of the spectrum. The commercially available version of EYFP from Clontech has also been codon-optimized to allow more efficient translation and higher expression levels in eukaryotic cells. EYFP is bright, with a high absorption coefficient of 83,400 M^{-1} cm^{-1} and a quantum yield of 0.61 [63]. It has been widely used to track the movement and distribution patterns of single proteins molecules on the membrane of live cells [76,94–96]. However, its high pKa (6.9) and sensitivity to halides cause its fluorescence to fluctuate in a cellular environment, where usually pH is 6.8–7.3 and Cl^- concentration is 10–60 mM [97,98]. In addition, EYFP is a weak dimer, with a K_d of 0.11 mM [99], although this should not be of significant concern for single-molecule studies. This is because most of the time, to achieve single-molecule detection in live cells, FPs are usually expressed at concentrations far below those required for significant dimer formation. A true monomeric YFP (mYFP) was generated by introducing the mutation A206K, in which the positive charge of the lysine side chain disrupts the hydrophobic interaction at the dimeric interface. The spectral properties of mYFP are essentially the same as those of EYFP.

Citrine

By introducing one additional mutation, Q69M, into EYFP, a new YFP named Citrine was generated, Citrine has a lower pKa at 5.7, is less sensitive to halide, and is about twice as resistant to photobleaching as EYFP [73,100]. The low pKa and insensitivity to halide could be explained by the Q69M mutation. The side chain of the Met was shown in the crystal structure to occupy a halide-binding cavity near the fluorophore, shielding the fluorophore from Cl^- or protons. The resistance to photobleaching may also be a direct result of the elimination of the cavity near the fluorophore, so that the fluorophore is better packed and shielded from the environment. Like its parent EYFP, Citrine is also a weak dimer, but its monomeric version was easily generated by introducing the same mutation A206K, and the resulting mCitrine has the same spectroscopic properties [73,75,100,101].

Venus

A particularly notable and popular YFP mutant is the fast-maturing Venus generated by the Miyawaki group [83]. Venus has comparable brightness, low pKa, and insensitivity to halide to those of mCitrine, but its most distinguishing feature is its fast fluorophore maturation process, the time constant of which is measured to be about 2 min *in vitro* [83] and 7 min inside live *E. coli* cells [84]. The accelerated fluorophore maturation results from a combined effect of the five point mutations (F46L, F64L, M153T, V163A, S175G), which likely introduce structural flexibility, remove steric and energetic constraints in the folding of the polypeptide chain, and enhances oxygen access to the fluorophore [83,102]. Given that many other FPs mature on the time scale of a few tens of minutes or hours, the accelerated maturation time of Venus is particularly attractive for monitoring cellular processes with fast dynamics such as gene expression. In a recent work by the Xie group, Venus was used as a single-molecule gene expression reporter to probe the real-time dynamics of a repressed *lac* promoter in live *E. coli* cells [84]. Had a FP with slower maturation kinetics been used in this work, the detected FP molecules generated from one single mRNA would have a much wider distribution in time, rendering it difficult to discern when an mRNA molecule was generated. One drawback of Venus is its low photostability—it photobleaches at least twice as fast as mCitrine. Therefore, Venus is not the best fluorophore to use in experiments such as

single-molecule tracking where photostability is crucial. Venus is also a weak dimer, but, just as in the cases of mYFP and mCitrine, an A206K mutation generates monomeric mVenus [101].

Yellow-Fluorescent Protein for Energy Transfer

Yellow-fluorescent protein for energy transfer (YPet) was originally generated during a screening for improved fluorescence resonance energy transfer (FRET) between CFP and YFP [103], but it was later found that the improved FRET performance of YPet is likely due to its tendency to dimerize with its coevolved partner CyPet [104,105]. Nevertheless, YPet is superior for single-molecule imaging because it is the brightest YFP available, with a very high absorption coefficient at 104,000 M^{-1} cm^{-1} and a quantum yield of 0.77. It was based on another bright YFP variant, Topaz [63], which was the brightest YFP before the appearance of YPet. Multiple mutations were introduced into Topaz through random mutagenesis, and the roles of many of them in improving its brightness are unclear. The maturation kinetics of YPet is similar to that of EYFP, but its photostability has not been addressed. There is no report on the use of YPet in single-molecule studies, but given its brightness and low pKa (5.6), its use in single-molecule imaging in live cells should be imminent.

3.5.2. Orange- and Red-Fluorescent Proteins

Fluorescent proteins that excite and emit at longer wavelengths than GFP or YFP are highly desirable for single-molecule imaging in live cells for three reasons. First, excitation at long wavelengths avoids exciting the flavin protein, which is the major source for high cellular autofluorescence background in the 500-to 600-nm region. Second, orange or red excitation in general causes less photodamage to cells because blue or green excitation carries more energy and can be absorbed by DNAs and proteins. Therefore, longer time traces can be obtained without exposing cells to severe photodamage. Third, RFPs can be spectrally distinguished from GFPs or YFPs, making it possible for two-color, single-molecule imaging in live cells.

Earlier efforts to engineer jellyfish avGFP to produce variants in the orange or red region had been unsuccessful,[4] although blue light–induced conversion from green to red fluorescence under limited oxygen supply had been reported [107,108]. This situation did not change until 1999, when the first RFP, dsRed, was discovered in a nonbioluminescent reef coral species, *Discosoma striata*, commonly called the striped mushroom [109]. This breakthrough started the second round of extensive mutagenesis efforts to improve the original dsRed because it matures slowly ($t_{1/2} = 27$ hr) through a green intermediate [110], has dim fluorescence [109], and is an obligate tetramer [110]. The results were successful, and a series of monomeric RFPs called mFruits were generated by the Tsien group [85]. Together with RFPs generated from other research groups and companies, there are now FPs ranging from orange to far infrared with much improved biochemical and photochemical properties (Figure 3.3) (also see comprehensive reviews in Refs. 75 and 101).

The formation of these RFP fluorophores (Figure 3.4) shares similar steps with GFP maturation but includes additional chemistry, which explains why the efforts to engineer

[4] There is one recent study reporting the generation of the first red fluorescence-emitting derivative (excitation and emission maxima at 555 and 585 nm, respectively) of avGFP [106]. Purified proteins or cells expressing this mutant, however, showed both green (strong) and red (dim) emission. It is likely that only a small population of the mutant matures to the red chromophore. Nonetheless, this study indicates that the full mutagenesis potential of GFP has yet to be reached.

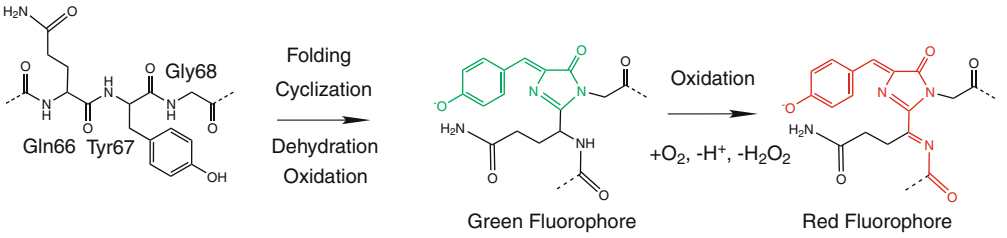

Figure 3.4. Maturation of the fluorophore in *Discosoma striata* red-fluorescent protein (dsRed) [112,113]. The first step is to form a green-emitting fluorophore as in green-fluorescent proteins through cyclization, dehydration, and oxidation, and the second step involves oxidation of the bond between the α-carbon and the nitrogen of Gln66 to form an acylimine, which extends the π-conjugation system.

avGFP to produce variants in the red region have been unsuccessful [111–113]. For dsRed, the initial steps also involve a tripeptide (Gln66, Tyr67, and Gly68) to go through similar cyclization, dehydration, and oxidation to form a coplanar *p*-hydroxybenzylidene-imidazolinone π system like that in GFP. However, additional oxidation at C_α—N bond of Gln66 takes place to form an acylimine group, leading to an extended π-bonding resonance system. This extended conjugation system results in greater delocalization of electrons upon excitation, giving rise to the longer excitation and emission wavelengths (558 and 583 nm, respectively). In addition to this extra oxidation step, the Phe65 and Gln66 of dsRed are connected by an unexpected and unique *cis* peptide bond, the isomerization of which from the usual *trans* bond formed initially upon protein folding is believed to be a key step that slows down the maturation of the fluorophore [112,114]. In other RFPs that derived based on dsRed, such as mOrange, mCherry, and mStrawberry, the fluorophores may undergo further chemical transformations [115]. In the following, a few OFPs and RFPs with promising potential for single-molecule imaging in live cells are discussed.

The brightness of OFPs and RFPs is usually less than that of the YFPs; however, as the cells' autofluorescence background is much less at the longer wavelengths, the slightly decreased brightness does not pose a significant problem for single-molecule imaging. In fact, mCherry, the dimmest among the few selected RFPs to be discussed, has been demonstrated to be detectable as single molecules in live bacteria cells [116]. Since many of the OFPs and RFPs to be described were just discovered very recently, some of their properties, such as fluorophore structures, maturation kinetics, photobleaching, and fluorescence-blinking behaviors, have not been fully characterized. Therefore, the following selection of FPs is based on the best knowledge available and serves as a starting point for further detailed investigations, especially at the single-molecule level.

Monomeric Orange-Fluorescent Protein Kusabira-Orange

The orange-fluorescent protein Kusabira-Orange (KO) was originally cloned from stony coral and selected as a FRET partner with CFP [117]. Because KO exists in the heterogeneous oligomeric state including dimers and tetramers, extra rounds of mutagenesis were carried out to introduce more than 20 mutations to generate the monomeric version mKO. mKO absorbs strongly at 548 nm, with a small shoulder at 515 nm, and emits maximally at 561 nm. Its overall brightness is comparable to that of EGFP, and its photostability appears to be better than that of many FPs, making it an attractive fluorescent label especially in single-molecule

tracking experiments [66,75]. mKO behaves well when fused to most proteins tested, although it was reported to cause problems in the localization of α-tubulin. Adding longer/flexible linkers or the N- or C-terminus of GFP to mKO may lessen this problem [66].

mOrange and mOrange2

mOrange (excites and emits maximally at 548 and 562 nm, respectively) was created during one substantial effort of reengineering dsRed and its derivatives to generate a series of orange- and red-emitting FPs called mFruits. Each FP in this series is named after a similarly colored fruit [85]. mOrange is the brightest monomeric FP in this series, but it photobleaches quickly. In addition, its pKa of 6.5 may pose a disadvantage compared to other mFruits, which usually have pKa values around 5 or lower. The absorption spectrum of mOrange has a minor peak at 470 nm, and it has a 510-nm emission peak under 470-nm excitation. This likely represents a population of fluorophores whose maturation stalls at a GFP-like fluorophore stage [118]. This can be a serious drawback in using mOrange in two-color imaging experiments. Work aimed at improving the photostability of FPs led to a new version, mOrange2, with four mutations that may hinder a critical oxidation reaction and loss of fluorescence of the fluorophore [66]. mOrange2 is less bright than mOrange but still compares favorably to other mFruits. The absorbance spectrum of mOrange2 has the similar additional peak around 490 nm, but excitation at this peak does not produce fluorescence. The most distinctive property of mOrange2 is its photostability, which is significantly (>25-fold) improved over that of mOrange and is among the best of all available FPs. However, its sensitivity to pH is not changed, and mOrange2 appears to mature twice as slowly as mOrange (4.5 instead of 2.5 hr).

tdTomato

The tandem dimer tdTomato is the brightest of all available FPs; it was created by fusing two copies of the dimeric dTomato gene, and thus possesses two bright fluorophores. Its excitation and emission wavelengths (554 and 581 nm, respectively) are red-shifted compared to those of mKO and mOrange, and it is also very photostable. The major drawback of its use in tagging proteins of interest is its relatively large size, which has been problematic when it was fused to α-tubulin and connexin, where tight packing of these fusion proteins is needed [66]. However, this should be case dependent, in that its fusion with myosin light chain appears to be successful [119]. Therefore, tdTomato fusion proteins need to be more carefully scrutinized for their functionality before any meaningful conclusion is drawn.

TagRFP and TagRFP-T

TagRFP-T is the optimized, monomeric version of the early tetrameric eqFP578 cloned from sea anemone [120]. TagRFP possesses a high absorption coefficient (100,000 M^{-1} cm^{-1}) and an intermediate quantum yield (0.48), with excitation and emission maxima at 555 and 584 nm, respectively. Of interest, the fluorophore of TagRFP, which is formed by the Met-Tyr-Gly triad, likely adopts a coplanar but *trans* conformation as in its homolog eqFP611 cloned from the same species [121]. This is different from the fluorophore conformations of the majority of other FPs, which are usually in the *cis* form. In addition, as will be discussed later for photoinducible FPs (PI-FPs), a mechanism of *trans*-to-*cis*

isomerization of the fluorophore is suggested to account for the photoinduction of the PI-FPs from the nonfluorescent to a fluorescent form. It is not clear why the *trans*-fluorophore of eFP611 is still highly fluorescent and how its conformation contributes to its photophysical properties.

Although TagRFP already possesses reasonable photostability, the Tsien group further optimized TagRFP by selecting mutants that exhibit prolonged fluorescence after intense photobleaching [66]. One mutation, S158T, was found to enhance the TagRFP's photostability ninefold. This new version, named TagRFP-T, is the most photostable FP across all spectral classes available, although its brightness is 20% lower than that of TagRFP. In addition, the absorption spectrum of TagRFP-T does not have other minor peaks that absorb but do not fluoresce, indicating that the fluorophore only exists in one fluorescent state.

mKate

The RFP mKate is also derived from eqFP587, the same progenitor as that of TagRFP [122]. In the red and far-red region where most RFPs are dim, mKate performs reasonably well, with an extinction coefficient of 45,000 M^{-1} cm^{-1}, a quantum yield of 0.33 (excitation and emission maxima at 588 and 635 nm, respectively), and a brightness that is comparable to that of mCherry. mKate also demonstrates high photostability, which is in the same range as that of the two newly developed OFP variants mOrange2 and TagFP-T. However, its photobleaching curve measured in ensemble exhibits complex behaviors, with an initial rise of fluorescence intensity followed by gradual decay, which was suggested to resemble that of photoinducible FPs. It is likely that some mKate molecules that originally exist in a dark state can be irreversibly driven into the bright state by intense laser irradiation at its absorption maximum, and continuous irradiation eventually leads to complete photobleaching. Further investigations, especially at the single-molecule level, are needed to characterize this photobleaching behavior.

mCherry

Another RFP, mCherry, has been one of the most promising RFPs in the mFruits series, in that it has exceptional photostability, its excitation and emission wavelengths are red-shifted further to around 600 nm, and it matures relatively rapidly [85]. Although its brightness is among the dimmest of the FPs selected in this chapter, its single-molecule detection has been realized in live bacterial cells [116]. Compared to mCherry, the newly developed mKate emits in the same far-red region, has similar brightness, and has better photostability. However, because the complex photobleaching behavior of mKate is not well characterized, mCherry remains a good fluorescent label to use in single-molecule imaging in live cells.

3.5.3. Photoinducible Fluorescent Proteins (PI-FPs)

Recent advances in FP engineering have resulted in another exciting class: the photoinducible FPs (PI-FPs).[5] This new class of FPs (Table 3.3) possesses a unique property in

[5] Here the term "photoinducible FPs" is introduced to characterize the common feature of this class of fluorescent proteins: They all undergo light-induced processes to change their fluorescence emission properties. In the literature, the terms photoactivation, photoswitching, and photoconversion are used, sometimes interchangeably. In the context of this chapter *photoactivation* refers specifically to the process of fluorescence turn-on from a dark state

that they undergo pronounced light-induced spectral changes in response to irradiation at a particular wavelength. This remarkable property enables their fluorescence to be controlled at will and is especially suitable for selectively marking macromolecules of interest in space and time and tracking their movement and redistribution inside a cell. For example, a protein can be labeled with a PI-FP, expressed at high density (10^5 molecules/μm^2) inside a cell. This high expression level still contributes minimally to the background, in that most of the PI-FP molecules are kept at the fluorescence off-state. Upon the application of photoinduction at a certain level, a few PI-FP molecules are selectively induced to become fluorescent, enabling single-molecule detection, localization, and tracking. These molecules can then be turned off by photoinduction or bleaching to allow the next round of recording. Thus, thousands of cycles can be carried out in the same cell to generate a large amount of data, facilitating statistical data analysis [123,124].

Available PI-FPs can be divided into two categories. The first category includes PI-FPs whose excitation/emission spectra are constant but whose fluorescence on- or off-state is changed by photoinduction. This category includes the photoactivatable RFP PA-mRFP1-1 [125], the photoswitchable RFP asFP595 [126], and the GFP Dronpa [127]. The second category includes PI-FPs whose excitation/emission color is changed by photoinduction. Typical examples are the irreversible, green-to-red photoconvertible FPs Kaede [128], KiKGR [129], EosFP [130], and Dendra [131] and the cyan-to-green PS-CFP [132]. Comprehensive reviews on the PI-FPs are available [101,133–135], and readers are directed there for the complete coverage of available PI-FPs. The focus here is on the PI-FPs that have the potential for or have already been demonstrated in single-molecule imaging in live cells. These PI-FPs include the photoswitchable Dronpa together with its derivative, the fast-switching rsFastlime; the newly developed rsCherry and rsCherryRev; the green-to-red photoconvertible monomeric mEosFP; and the improved version of Dendra, Dendra2. All of these PI-FPs are monomeric and possess sufficient brightness to be imaged at the single-molecule level. Their spectral properties are summarized in Table 3.3.

Many members in the GFP, YFP, and RFP classes also exhibit similar photochromatic behavior, although the photoinduction quantum yields are usually much lower than that of PI-FPs [66,68,77,79, 80,136,137]. Some molecules that appeared to be “photobleached” are actually molecules that stayed in long-lived dark states. These molecules can be photoinduced to fluoresce again with illumination with violet or blue light. The mechanisms of their switching in general may be similar to that of the PI-FPs, as discussed later.

Dronpa and Its Derivative rsFastLime

Dronpa and its derivatives are the best-studied PI-FPs [127,138]. Their fluorescence can be detected with blue excitation (488 nm), but prolonged blue excitation will drive Dronpa into a dark state (switch-off). Dronpa can escape from the dark state by irradiation of violet light (405 nm) to become fluorescent and detected by 488-nm excitation again (switch-on). This switching-on and -off cycle can be repeated more than 100 times for a single Dronpa molecule imbedded in polyvinyl alcohol film before it finally photobleaches [138].

The photoinducible switching between the on- and off-states of Dronpa is likely due to the light-induced fluorophore protonation state and/or conformational changes [138–144].

irreversibly (off → on); *photoswitching* to the process of reversible fluorescence turn-on and turn-off cycles (off ↔ on); and *photoconversion* to the process of light-induced change of excitation/emission spectra between two color regions (on_1 on_2).

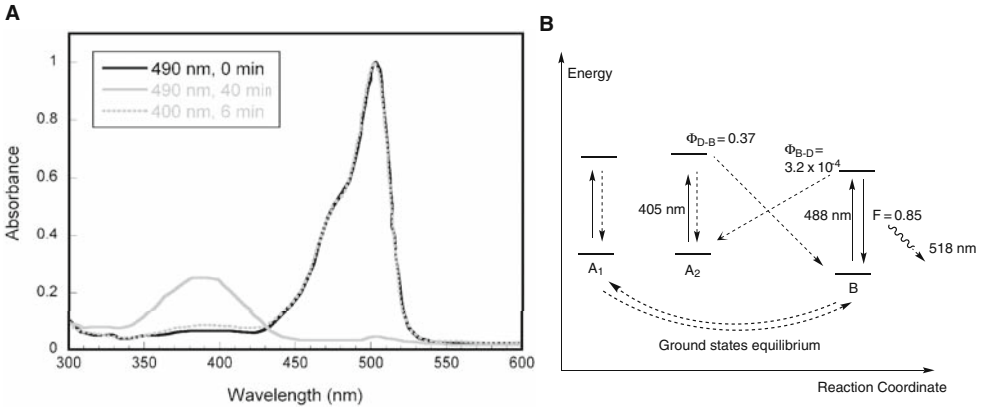

Figure 3.5. A. Absorption spectra of Dronpa before 490-nm illumination (*black*), followed by 490-nm illumination for 40 min (*gray*) and then after 400-nm illumination for 6 min (*dotted gray*) The three curves exhibit an isosbestic point at 428 nm. Irradiation at 490 nm for a prolonged time completely diminishes the absorption peak around 500 nm and increases the population that absorbs at 390 nm. Brief irradiation at 405 nm completely restores the 500-nm peak and diminishes the 390-nm peak. (Adapted from Ando et al. [127].) **B.** Proposed photoswitching states of Dronpa. Form B is the deprotonated form, which can be excited at 488 nm to emit fluorescence; A_1 is the protonated form, which exists in equilibrium with form B through ground-state deprotonation and protonation and does not fluoresce; A_2 is the protonated form, which only forms through the excited form B and cannot relax spontaneously to B but can be converted to B through irradiation at 405 nm.

Dronpa's absorption spectrum (Figure 3.5A) has one major peak at 503 nm and a minor one at 390 nm, corresponding to the deprotonated (B) and neutral (A_1) forms of the fluorophore, respectively (Figure 3.5B). Only the deprotonated form B is fluorescent upon excitation at 488 nm (emission peak at 518 nm, with quantum yield Φ of 0.85). When Dronpa is illuminated at 488 nm for a prolonged time, the deprotonated form B undergoes an efficient ESPT from the excited state to a protonated ground state (A_2), which is not fluorescent. This constitutes the switching-off of the photocycle of Dronpa, with a switching quantum yield $\Phi_{B\cdot D}$ of about 3×10^{-4}. The protonated form A_2 relaxes very slowly (days) to the deprotonated form B, is different from the originally neutral form A_1, which exists in equilibrium with the deprotonated form B, and, most remarkably, can be rapidly (within milliseconds) converted to the deprotonated form B by 405-nm irradiation (Figure 3.5B). The conversion of A_2 to B constitutes the switching-on of the photocycle because after 405-nm irradiation, bright fluorescence is regenerated with 488-nm excitation. The quantum yield for the switching-on $\Phi_{D\cdot B}$ is very high (~ 0.37). The on-time, that is, the time for a single Dronpa molecule to stay at the deprotonated form B during 488-nm illumination, is linearly dependent on the excitation power in the range tested (0.2–3 kW/cm^2)—the higher the power, the shorter is the on-time. Similarly, Dronpa's switching-on rate is also power- dependent, with stronger 405-nm irradiation giving higher switching-on rates [145].

Structural studies using X-ray crystallography and nuclear magnetic resonance (NMR) confirmed that the fluorophore, formed by the Cys62, Tyr63, and Gly64 tripeptide, is deprotonated in the bright state and protonated in the dark state [140,141,144]. In addition, these studies also suggested that conformation changes in the fluorophore, such as a *cis–trans* transformation as in asFP595 [140], the overall β-barrel structure flexibility [144], and/or the

extensive hydrogen-binding network of the fluorophore with surrounding polar groups [141] contribute to light-induced photoswitching.

Dronpa has been successfully applied to probe the shuttling of signaling molecules between different cellular locations and track cell fates using whole-cell labeling at the ensemble level [127,146–148]. It also has been detected at the single-molecule level *in vitro* [138,142,149] and in fixed cells [150]. However, its imaging at the single-molecule level in live cells has not been reported. Based on Dronpa's high quantum efficiency (0.85) and high absorption coefficient (95,000 M^{-1} cm^{-1}), it is the brightest FP among the selected PI-FPs and there is no reason why its single-molecule imaging in live cells cannot be done. The only drawback, however, could be the reported residual fluorescence when Dronpa is in the off-state (10% of its on-state fluorescence measured at the ensemble level [151]). Therefore, it may be difficult to image single Dronpa molecules in a densely labeled cellular environment because the residual fluorescence of Dronpa molecules in the off-state will contribute to a high background. It is not clear whether the residual fluorescence of Dronpa in the off-state is an intrinsic property of the fluorophore or whether 488-nm irradiation can also switch on Dronpa molecules in the off-state (although inefficiently), creating a dynamic equilibrium between Dronpa molecules in the off- and on-states.

Further engineering of Dronpa produced three mutants that accelerate the switching between the bright and dark states, possibly by reducing the steric hindrance of fluorophore conformational changes [140]. One of these, the V157G mutant rsFastLime, has a good combination of brightness and fast switching kinetics (faster switching-off and spontaneous switching-on rates) (Table 3.3). The other two mutants, M159T and M159S, although switching much faster, are both too dim to be useful in single-molecule imaging in live cells. The fast switching-off property of rsFastLime has been successfully used in photoactivated localization microscopy (PALM) in fixed cells to shorten the imaging time from more than 10 hr to a few minutes [152]. In single-molecule tracking experiments, however, the fast switching-off property of rsFastLime does not necessarily pose an advantage over Dronpa because it causes short fluorescence on-times, limiting the duration of tracking trajectories. However, the spontaneous switching-on property of rsFastLime simplifies instrumentation because only one laser line (488 nm) rather than two alternating lines (488 and 405 nm) satisfies both the switching-on and -off requirements, although the addition of a 405-nm line significantly enhances the switching-on probability.

rsCherry and rsCherryRev

The newest additions to the reversibly photoswitching FP family are the red-emitting rsCherry and rsCherryRev, which were semirationally derived from mCherry [153]. By incorporating into mCherry mutations that likely facilitate *cis–trans* transition and modify the immediate hydrogen-bonding environment of the fluorophore, rsCherry and rsCherryRev were produced with opposite photoswitching properties. In the on-state, both FPs absorb and emit maximally around 570 and 610 nm, which are slightly blue-shifted compared to mCherry. Prolonged illumination using a yellow light (550 nm) turns off rsCherryRev, just as Dronpa is reversibly inactivated on prolonged illumination at its detection light (488 nm). For rsCherry, however, the same yellow light illumination switches on its fluorescence from its dark state. Similarly, blue light (450 nm) has the opposite effect on the two proteins—it turns on rsCherryRev but turns off rsCherry. The brightness of these two proteins is reported to be similar to that of mCherry based on FCS measurements, rendering their single-molecule

detection achievable in live cells. Indeed, rsCherryRev has been applied successfully to live mammalian cells, in which single-molecule, superresolution imaging with a 70-nm spatial resolution was achieved [153].

EosFP

EosFP was cloned from the stony coral *Lobophyllia hemprichii* in 2004 [130]. It was named after Eos, the goddess of dawn in Greek mythology, "who brings light to all the mortals of this earth" (Hesiod, *Theogony*), as it changes its color from green to red irreversibly on violet irradiation. EosFP was first isolated as a tightly associated tetramer but was eventually engineered to be a monomer (mEosFP) by breaking the interfaces of subunits in a similar way to that of DsRed [154]. mEosFP has similar spectral properties and brightness to those of EosFP but was reported to fold poorly in mammalian cells at 37°C [130]. This presents an obstacle for live-cell imaging at the ensemble level but may not have significant adverse effect for live-cell imaging at the single-molecule level because only folded and fluorescent molecules will be selected and imaged. Another way to circumvent this is to use a tandem dimer tdEosFP in which two subunits are connected through a flexible linker sequence, which expresses well at 37°C [155].

The crystal structures of EosFP in the green and red states have been elucidated (Figure 3.6) [156]. The fluorophore of EosFP is formed by the His62-Tyr63-Gly64 tripeptide. In its green-emitting state, the fluorophore is the anionic hydroxybenzylideneimidazolinone, the same as that of a typical GFP. This anionic fluorophore absorbs and emits maximally at 505 and 516 nm, respectively, with a fairly high absorption coefficient ε of 72,000 M^{-1} cm^{-1} and a quantum yield Φ of 0.7 (the ε and Φ of mEosFP are similar to those of EosFP). On irradiation around 390 nm, the fluorophore undergoes a peptide backbone breakage between the N_α and C_α atoms of His62 via a β-elimination mechanism [157], resulting in two peptide fragments (8 and 20 kD, respectively) that still bind to each other to form the β-barrel structure but separate on denaturing gel electrophoresis [130]. The reaction is likely mediated by Glu212 and Phe61, in which Glu212 may act as a base to extract one proton from the C_β atom of His62, whereas the imidazole ring of His62, which is transiently protonated during photoinduction, simultaneously donates a proton to the Phe61 carboxyl, making the peptide bond between Phe61 and His62 an ideal carboximidic leaving group in the elimination reaction. After the leaving of Phe61, the π-bonding system extends to the imidazole ring of His61 via a *trans*-alkenylene and forms the red-emitting fluorophore with shifted absorption and emission maxima at 569 and 581 nm, respectively.

It is noteworthy that the initial substrate for photoconversion is the protonated instead of deprotonated fluorophore, as evidenced by the drastically increased yield of photoconversion at low pH. This property may be used to one's advantage when imaging EosFP in an acidic environment such as the early endosomes.

The photoconverted mEosFP is about half bright after conversion, but because it emits in the red region where cells' autofluorescence is also reduced, single-molecule detection of EosFP in live cell is still possible. Indeed, the tandem dimer tdEosFP has been used successfully in single-molecule tracking in live cells [123]. Because of its photoconvertibility and the high contrast ratio between the converted and unconverted forms, thousands of single-molecule tracking trajectories can be obtained from a single cell by alternating the converting and detecting laser beams [123]. In another study, tdEosFP was paired with Dronpa in a clever imaging sequence to demonstrate dual-color PALM imaging [158]. Although this work was

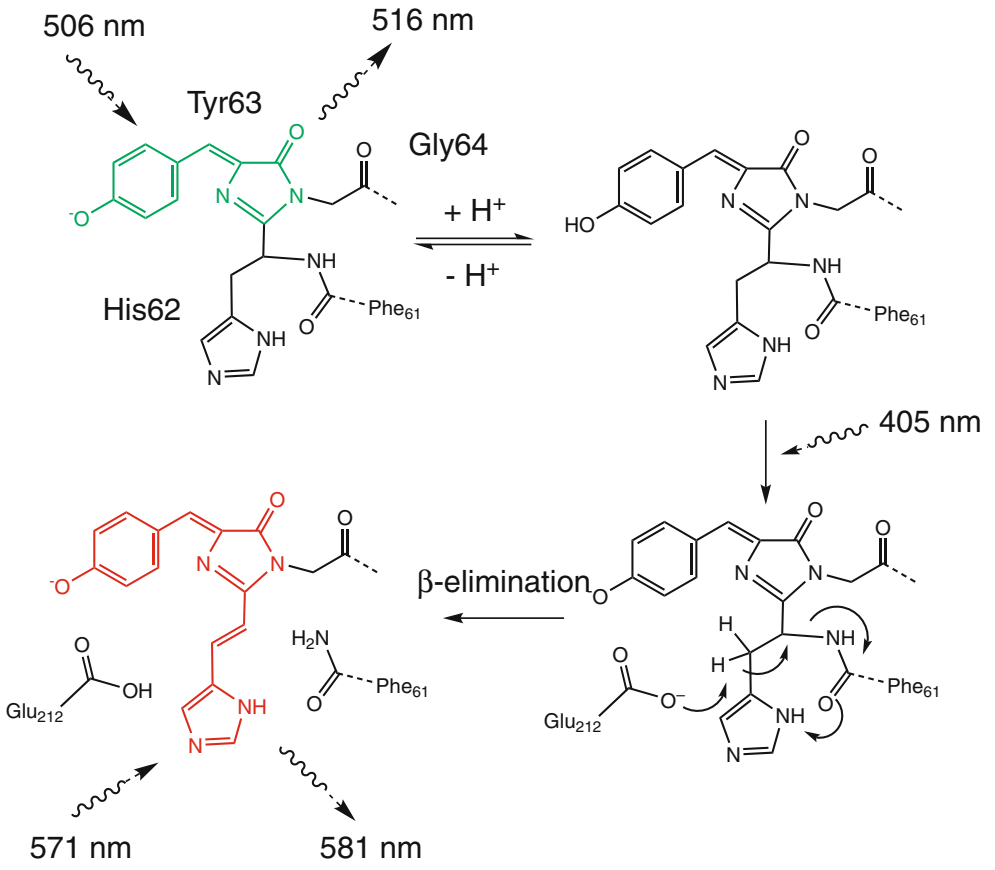

Figure 3.6. Proposed mechanism for the photoconversion of EosFP from its green form to red form. (Adapted from Nienhaus et al. [156].)

carried out in fixed cells and the overlapping green emission of tdEosFP before conversion in Dronpa's channel does not allow simultaneous imaging of both proteins in densely labeled live cells, it demonstrated that Dronpa and photoconverted tdEosFP have little spectral crosstalk and that EosFP has the highest contrast ratio between its photoinduced and noninduced forms compared to other PI-FPs including Dronpa, PA-GFP, and PA-CFP, making it an attractive probe [158].

Dendra2

Dendra2, the improved version of the monomeric fluorescent protein Dendra, is a recent addition to the PI-FP family [131]. Dendra2 is similar to mEosFP in that it can be converted irreversibly from a green-emitting species (excitation and emission maxima at 490 and 507 nm, respectively) to a red-emitting one (excitation and emission maxima at 553 and 573 nm, respectively). Denra2 differs from mEosFP in that its photoconversion can be mediated both by intense blue light irradiation of 488 nm and violet light irradiation of 405 nm; the latter is usually the only workable light source for photoconversion of many other PI-FPs,

including EosFP. Because the fluorophore of Dendra2 is formed by the same His-Tyr-Gly tripeptide, the photoconversion mechanism mediated by 405-nm irradiation is thought to be similar to that of EosFP. However, it is not clear what the mechanism is underlying the 488-nm blue light–mediated photoconversion because no crystal structure of Dendra2 is available. The use of 488-nm light to induce the green-to-red conversion of Dendra2 poses less toxicity to the cells than the 405-nm light, but high power, usually in the range of a few hundred W/cm^2, is required. Dendra2 is reported to express well in both bacterial and mammalian cells at 37°C, indicating efficient folding and fluorophore maturation processes. Although the overall brightness of Dendra2 before and after conversion is slightly less than that of EosFP, it has been successful imaged in live bacterial cells at the single-molecule level [159].

3.6. Special Considerations for Live-Cell Imaging

To achieve single-molecule detection in live cells, the main challenge is to enhance the signal-to-noise ratio by decreasing the cellular autofluorescence background and/or increasing detectable fluorescent signal. In addition, photodamage caused by laser exposure has to be carefully minimized to ensure a normal physiology of cells throughout an experiment.

3.6.1. Autofluorescence

The main hurdle in detecting single molecules in live cells is the background due to the intrinsic cellular fluorescence (autofluorescence). In bacterial cells, autofluorescence is usually homogeneous and diffusive, while in mammalian cells autofluorescence is heterogeneous, with most of the autofluorescence coming from various organelles such as mitochondria in the cytoplasm, although it is absent from the nucleus [160]. The strength of autofluorescence is also dependent on cell type, with microphages, neurons, and sperm cells exhibiting particularly strong autofluorescence.

The main sources of autofluorescence are nicotinamide adenine dinucleotide phosphate [NAD(P)H] between 400 and 500 nm and flavins and flavoproteins between 500 and 600 nm. Their emission levels are dependent on the local environment, cell type, growth condition, and cell physiology [160–162]. To increase the detectability of a single fluorophore above the autofluorescence background in the visible region, the most important tactic is to choose a fluorophore with red-shifted spectra compared to that of flavins whenever possible. The top panel of Figure 3.3 shows the excitation and emission spectra of flavin adenine dinucleotide (FAD). It is evident that by red-shifting excitation beyond 500 nm, autofluorescence from flavins can be greatly reduced. Therefore, YFPs and RFPs are much more suitable than GFPs for single-molecule imaging in live cells. One should also keep in mind that flavins exist at high concentrations inside cells (10^7 molecules/cell [162]); even excitation at the tail region of its excitation spectrum will generate a large fluorescence background and could easily overwhelm the signal from a single FP molecule. Therefore, it is necessary to further minimize the autofluorescence background of cells. Because NAD(P)H, flavins, and flavoproteins are essential cellular components, it is difficult to achieve background reduction by reducing their cellular levels and still maintain good cell physiology. Despite these difficulties, there are a few ways to alleviate the problem and allow single-molecule detection.

First, defined rather than complex medium usually works better for reducing cellular autofluorescence. For example, for bacterial cells, M9 instead of LB medium was found to reduce autofluorescence significantly [163]. For mammalian cells, Leibovitz's L15 medium

or Dulbecco's Modified Eagle Medium (DMEM) buffered with *N*-2-hydroxyethylpiperazine-*N*'-2-ethanesulfonic acid (HEPES) (no phenol red) has been used. For some cell types, certain media may induce high autofluorescence; therefore, different growth media should be tested prior to experiments. Second, cells under stressful, crowded, or otherwise poor growth conditions often have increased cellular autofluorescence [160, 163]; thus, keeping cells in a healthy growth condition is essential. Third, using a small excitation volume through the application of total internal reflection (TIR), confocal illumination or shrinking the wide-field illumination area can effectively reduce the background by reducing the number of autofluorescence-emitting molecules in the excitation volume. Fourth, cells can be prephotobleached to eliminate autofluorescence background before the collection of data. This is only applicable for short-term experiments because extensive prephotobleaching usually produces severe photodamage to cells. Finally, the emission fingerprinting mode offered by the Zeiss LSM META confocal microscope allows one to collect and resolve the spectra of fluorophores with closely overlapped emission at a relatively fast speed [164,165]. Although the detection of single molecules in this mode has not been realized (possibly due to the low detection efficiency of this commercial system), the basic principle of spectral instead of intensity separation holds promise for rejecting autofluorescence background from imaging fluorophores. In addition, it should be noted that although fluorescence lifetime gating has been suggested and successfully applied to separate autofluorescence and imaging fluorophores [76,166,167], this technique does not provide much advantage if the imaged fluorophores are FPs. This is because the fluorescence lifetime of FPs (~3 ns [76]) is not significantly different from that of flavins or flavoproteins (~1–5 ns [168, 169]).

3.6.2. Fluorescence Signal Enhancement

In addition to focusing on minimizing autofluorescence background, one should also consider enhancing the fluorescent signal from a given fluorophore. One way to achieve this is to spatially confine a fluorophore in a small region of the cell so that its diffusion is slowed down and its fluorescence is not spread over an area greater than a diffraction-limited spot during the acquisition time (usually in the range of a few tens or hundreds of milliseconds) [84,92]. An extension of this idea is the stroboscopic detection of a single RFP freely diffusing in the cytoplasm of *E. coli* cells using very high excitation power (~50 kW/cm^2) and short laser exposure time (0.3 ms) [116,170]. The high excitation power pumps the molecule as fast as possible so that a maximal number of photons are collected within the short period of laser exposure, during which the molecule has not moved so far as to produce a fluorescence image that is too spatially diffuse. Although it provides exciting possibilities for probing protein dynamics directly in the cytoplasm, brighter and more photostable fluorophores are needed because the intense pulsing of excitation often drives FP molecules into a dark state (blinking or photobleaching) [68,74] before enough photons are collected.

Another way to amplify a fluorescent signal is through the use of multifluorophore labeling of single macromolecules or enzymatic conversion of fluorogenic substrates [3,9,10,171,172]. For example, to observe the dynamics of a single chromosome molecule, an array of the binding site of the transcription factor LacI (96–256 copies) is integrated into the chromosome. On the binding of hundreds of GFP-LacI fusion protein molecules, a bright fluorescent locus is formed and serves as a marker to track the dynamics of the chromosome inside cells [6–8]. Similarly, by integrating 96 MS2 RNA-binding loops into an mRNA molecule and expressing MS2-GFP fusion proteins in the same cell, transcription can be monitored in real time in live cells and the subsequent transportation of mRNA

transcripts followed [3–5,173]. Another method is to use an enzyme that converts a fluorogenic substrate into fluorescent molecules at a high turnover rate, so that each enzyme molecule generates thousands of copies of fluorescent molecules, enabling the detection of single enzyme molecules in live cells [9,10]. These methods convert the challenging single-molecule detection into multifluorophore detection, making it easy for a biological lab equipped with a regular lamp-excitation fluorescence microscope to conduct investigations at the single-molecule level. However, the tagging of hundreds of copies of FP molecules on a chromosome or mRNA molecule may cause severe perturbation of the normal functions and cellular fates of these macromolecules [4,172], requiring extreme care for meaningful interpretation of experimental data. In addition, the enzymatic amplification method does not allow the imaging of the localization of enzyme molecules because the small fluorescent molecules diffuse quickly inside the cells and the spatial information is lost.

3.6.3. Laser-Induced Photodamage of Cells

Unlike fixed cell imaging, in which photobleaching is of major concern, in live-cell imaging, photodamage must be limited. Photodamage of live cells caused by laser illumination (Figure 3.7) is often observed as abnormal cell morphology, a granular appearance of the cell surface, a condensed nucleus, cell detachment, excessive vacuole formation, necrosis, arrested cell division, and, in some cases, sudden significantly enhanced cellular autofluorescence. Eventually, photodamage leads to cell death and prevents proper interpretation of imaging data. This is particularly detrimental in time-lapse imaging experiments, in which cells need to maintain their normal physiology for hours or even days.

The phenomenon of photodamage has been investigated, but its detailed mechanism is far from being conclusively determined. In general, the severity of photodamage of live cells is dependent on illumination wavelength, dose, and cell type—the shorter the wavelength, the higher the illumination dose, and the more fragile the cell type, the more severe is the damage. In the UV region, where nucleic acids and proteins absorb strongly, pyrimidine dimer formation, DNA strand breaks, and DNA–protein cross-linking caused by photon–DNA interactions have been reported [174–176]. In the near-infrared region (700–1100 nm), where high laser power density in the range of 10^7–10^8 W/cm^2 in optical-trapping and two-photo microscopy is used, laser-induced transient cell heating, two-photon absorption, and generation of reactive oxygen species (ROS) have been suggested to cause photodamage [177–180]. In the visible light region (500–600 nm), generation of ROS such as singlet oxygen and free radicals during photobleaching of excited biomolecules and fluorescent molecules has been documented [181–183]. This is especially problematic when high concentrations of fluorophores are used (Figure 3.7B, bottom panel). ROS may directly attack the lipid membrane, proteins, and nucleic acids through oxidative reactions [184] and perturb the cellular redox homeostasis through the accumulation of free radicals [185].

Because most single-molecule, live-cell imaging experiments are carried out in the visible region using a continuous wave (CW) laser that offers relatively low excitation power density (<1 kW/cm^2), and because FPs are usually expressed at very low levels, photodamage of cells is often minimal. Indeed, studies found that illumination of human lymphocyte cell cultures between 540 and 650 nm at low laser dose produces negligible photodamage [186] and that only when power exceeds 3.5 kW/cm^2 with 532-nm excitation do *E. coli* cells show appreciable damage [187].

One should still keep in mind that all cells are photosensitive, and free radicals generated through the photochemistry of excited fluorophores cannot be completely eliminated.

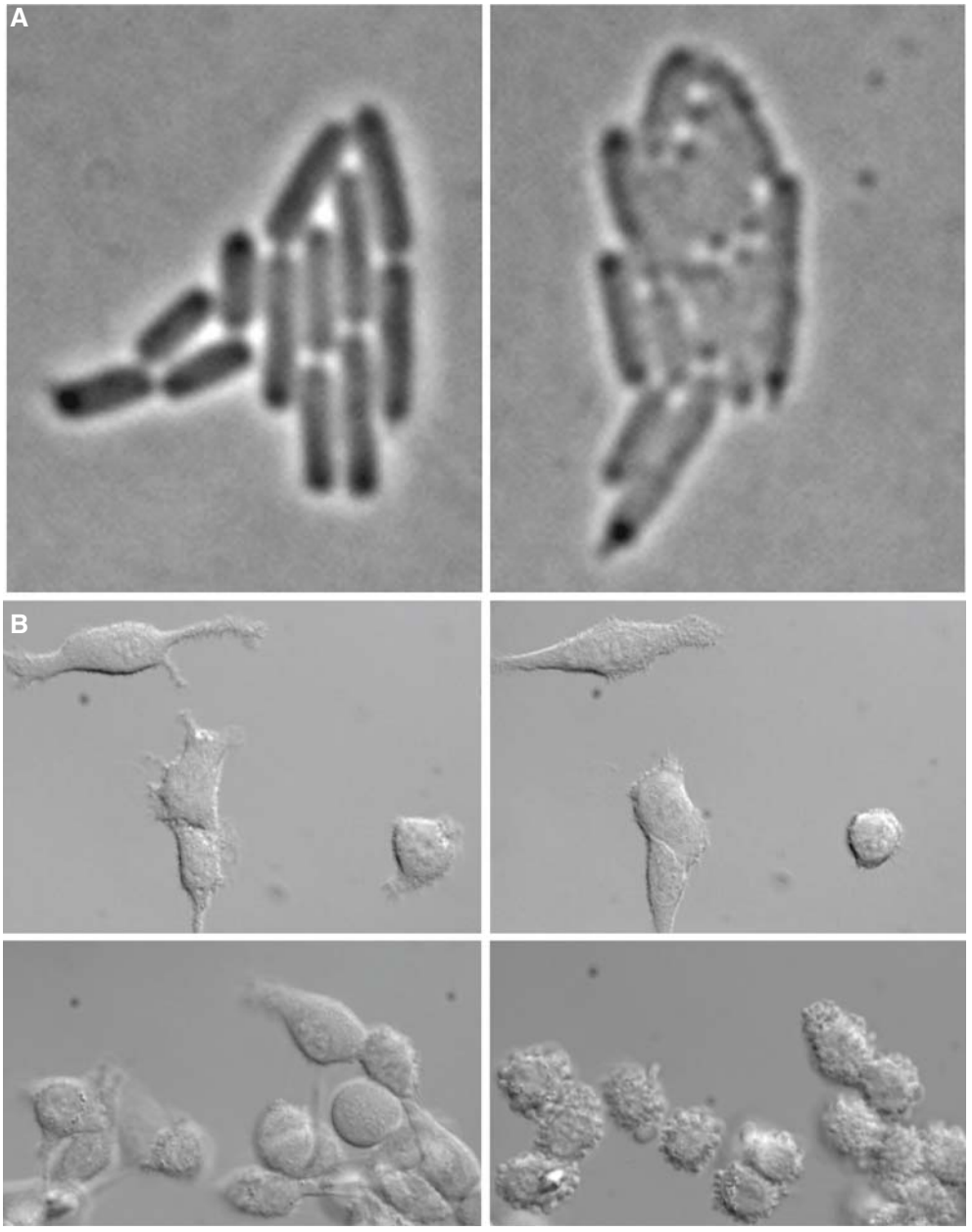

Figure 3.7. Effect of photodamage on live cells. Bright-field images of *Escherichia coli* cells (MG1655) (**A**) and mammalian cells (9L/LacZ, ATCC CRL-2200) (**B**) before (*left*) and after (*right*) prolonged laser illumination at 514 and 635 nm, respectively. Before laser illumination, cells appeared to have smooth cell surface and clearly defined edges. After laser illumination (514 nm, 0.6 kW/cm^2, 600 ms every 3 min for 3 hr), the photodamaged *E. coli* cells appeared to have blurred edges, dark spots, and rugged cell surfaces. The 9L/LacZ cells (**B, top**) did not show much morphology difference before and after laser illumination at 635 nm (0.4 kW/cm^2, 100-ms exposure every 20 sec for 120 min), except that cells were slightly bulged. In contrast, when cells (**B, bottom**) were loaded with 10 μM of dimethylacridinone (DDAO)-Gal (a fluorogeneic substrate of β-lactosidase) that was converted to highly fluorescent DDAO at high concentrations, cells showed severe photodamage, as evidenced by detachment, blebs, and shrunken cell sizes after illumination at the same condition for 70 min. This demonstrates the phototoxicity caused by the photochemistry of excited dyes.

Prolonged laser illumination, even at low power density and in the visible wavelength region, will produce enough free radicals that they will eventually exceed the buffering capacity of the redox system of cells and lead to severe photodamage of cells. A compromise between the best image quality and the health of cells must be reached. The most effective method of reducing photodamage is to use the lowest possible light intensity and to separate laser exposures widely during acquisition. This is because cell damage and free radical generation show a nonlinear relationship to the excitation light intensity, and high excitation intensities with brief exposure times promote greater damage to cells than low excitation intensities with long exposure times [183,188]. One should carefully adjust excitation light level and sampling rate to minimize the adverse effect of photodamage, and at the end of each experiment always compare cells that have and have not been subjected to laser exposures to determine whether significant photodamage has occurred.

3.7. Instrumentation

3.7.1. Illumination Source

Although single-molecule detection has been achieved using lamp excitation [189], a monochromatic and highly collimated laser beam is much preferred for single-molecule imaging experiments. Laser illumination offers advantages that cannot be matched by lamp excitation: It provides an extremely pure excitation wavelength, delivers high excitation power, and diverges very little during travel. The lasers most commonly used for single-molecule imaging in live cells are CW lasers, which produce a continuous beam output that has constant amplitude and frequency in time. CW lasers emitting in the blue, green, and yellow regions include gas lasers such as argon and krypton ion lasers, solid-state lasers such as diode lasers, and liquid lasers such as dye lasers. The major manufacturers for these lasers include Coherent, Inc., Spectra-Physics, and CrystaLaser. In Figure 3.3 the major lines of commercially available lasers are plotted along with the excitation spectra of commonly used fluorophores. Liquid dye lasers offer the flexibility of tuning excitation wavelengths continuously to match the excitation maxima of a fluorophore, but they generally require more maintenance than the gas or solid-state lasers because the dye needs to be changed frequently to ensure a constant power output. Pulse lasers, which generate intense laser pulses in milliseconds or femtoseconds, are used in multiphoton microscopy and are not discussed here.

The guidelines for selecting a suitable laser of excitation wavelength for single-molecule, live-cell imaging is not much different from that for *in vitro* single-molecule imaging. First, the laser wavelength should be close to the excitation maxima of a chosen fluorophore; in two-color imaging, the criterion is to minimize cross-talk of the two fluorophores while maximizing their excitation. Second, the laser power should be sufficiently high so that when a large illumination area is used an average excitation power density between 0.1 and 1.0 kW/cm^2 can still be achieved. Third, the laser should have a stable single mode with a Gaussian beam profile (TEM_{00}) so that the beam can be focused down to a diffraction-limited spot or expanded to illuminate a large area uniformly. Lastly, the laser should also have high pointing and power output stabilities, which is especially critical for long-time-lapse imaging of live cells. In addition, because the most popular fluorophores used in live-cell imaging are FPs, which are much larger than small-molecule organic dyes, their rotational movement inside cells may be slow and comparable to the imaging time scale. Therefore, the intensities of individual molecules will have large variations due to the relative orientations of their dipoles with respect to that of a polarized laser beam. These variations are larger than what

one would expect from pure photon statistics and sometimes make interpretation of single-molecule data difficult. To circumvent this problem, the linearly polarized incident laser beam can be converted to circularly polarized light by inserting a quarter-wave plate in the optical pathway. In some cases, the coherence of the laser beam is also scrambled to avoid speckle patterns in the imaging area due to the interference of the coherent laser beam by dust or surfaces of optics in the pathway [190].

3.7.2. Illumination Mode

To reduce background and enhance single-to-noise ratio in single-molecule, live-cell imaging, besides carefully prepared cell samples and selected optics, minimization of excitation volume is essential. Three illumination modes—wide-field, confocal, and TIR—are often used and discussed next (Figure 3.8). For the general principles of fluorescence microscopy, the reader should consult the textbook by Murphy [191].

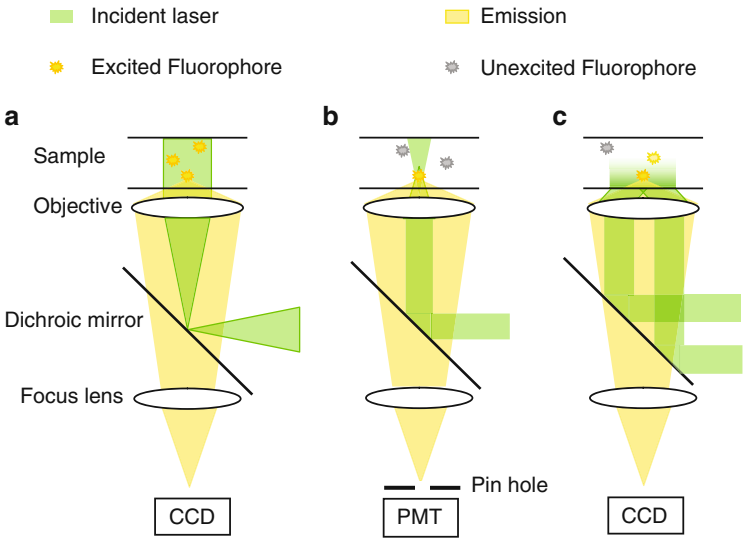

Figure 3.8. Schematic drawing of three illumination modes: wide field (**A**), laser scanning confocal (**B**), and objective-type total internal reflection (TIR) (**C**). The excitation beam is shown by green shading and the emitted fluorescence by yellow shading. Fluorophores that are in the excitation volume are shown as yellow stars, and the ones outside are shown in gray. In the TIR mode, the evanescent field is shown in gradient green color.

Wide-Field Illumination

Conventional wide-field illumination, in which a beam of collimated laser light is used to illuminate a large area of sample, is the most commonly used mode in fluorescence microscopy. It is easy to set up and often cost-effective compared to other illumination modes. It offers a large view field (up to the full size of a CCD chip) and allows simultaneous imaging of multiple molecules, improving data throughput. In single-molecule imaging, however, a smaller illumination area on the range of a few to a few tens of μm^2 instead of the full chip size is often used to minimize the background. In practice, a combination of lenses with different focal lengths is used to first expand and focus the laser beam to the back aperture of the

objective at a desired cone angle to reach an illumination area of 100 μm^2. Then an iris is used to cut off the fringe of the laser incident beam so that only the center area of about 20 μm^2 (or larger if cell size is larger) is used for imaging. This efficiently cuts down the background and ensures homogeneous excitation throughout the illumination area. The tradeoff of this configuration is obviously the reduced number of cells and molecules in the view field, which is easily compensated for by imaging multiple areas sequentially. A more serious drawback of wide-field illumination is that, for high–numerical aperture objectives, the depth of field where objects stay in focus is less than 1 μm; thus, for thick cells (5–30 μm) other fluorescent molecules above this 1 μm in the excitation path of the collimated laser beam will generate out-of-focus light and contribute to high background. Therefore, wide-field illumination is usually used for small and flat cells such as bacterial and epithelial cells.

Confocal Illumination

Confocal illumination effectively minimizes background signal by exciting a sample with a focused laser beam that has the dimension of a diffraction-limited spot, the smallest excitation volume achievable in far-field optical microscopy, and using a pinhole that is in an optically conjugate plane in front the detector to reject light below or above the focal plane of the objective. Because of the point excitation, illumination of a large area is achieved by scanning the area pixel by pixel through computer-controlled movement of the sample or laser beam, and fluorescence emission at each point is collected by a photomultiplier tube (PMT) through the pinhole. The output from the PMT is then built into an image according to their spatial positions and displayed by a computer.

Confocal illumination offers excellent ability in reducing background and generating high-contrast three-dimensional images, but it is not the best choice for single-molecule imaging in live cells. First, the point-scanning format renders a slow frame rate, typically at a few frames per second for a commonly used laser scanning confocal microscope (LSCM). Therefore, fast cellular dynamics at the millisecond time scale are not accessible. Shrinking the scanning area or reducing the dwell time of the laser at each pixel increases the frame rate to 20–30 frames/sec. However, this usually does not permit single-molecule detection because a laser dwell time of 0.1–1.0 μs/pixel at a single emitter in rapid scanning mode does not generate enough photons to distinguish the signal from background noise. Second, the PMT used in a confocal microscope has low quantum efficiency (0.5–0.6) for detecting photons, rendering single-molecule detection difficult.

A new format of confocal microscopy, spinning-disk confocal, also called Nipkow disk confocal [192,193], demonstrates improvements over LSCM, in that it offers relatively fast imaging speed. Spinning-disk confocal uses one disk carrying an array of spirally arranged microlenses to focus the laser beam onto a second disk carrying an array of pinholes arranged in the same pattern. The microlenses and pinholes are arranged in such a pattern that when the two disks spin at high frequency, they effectively split the excitation laser beam into thousands of beams, simultaneously illuminating every point of the imaging area; thus, a high imaging speed at 1,000 frames/sec can be achieved. In addition, a CCD camera instead of a PMT is used, so that the detection efficiency is also improved. Based on these techniques, spinning-disk confocal is a better choice over LSCM for single-molecule imaging in live cells, although the fluorescence signal is still reduced due to the splitting of the excitation light.

Total Internal Reflection Illumination (TIR)

TIR illumination offers the best combination of background reduction, wide-field data collection, and high imaging speed through the use of an evanescent field as the excitation source (Figure 3.9). The evanescent field is generated by the excitation laser beam traveling at a high incident angle at the interface between the glass coverslip and water. At a particular angle determined by the difference between the refractive indexes of glass and water, the light is totally reflected from the interface but generates a very thin electromagnetic field at the same frequency as the incident light in the water phase. This electromagnetic field is called the evanescent wave, and its intensity decays exponentially perpendicular to the interface with a distance dependence of

$$I_z = I_0 e^{\frac{-z}{d}}$$

where I_z is the excitation intensity at a distance z from the interface, I_0 is the excitation intensity at the interface, and d is the characteristic penetration depth, which is defined as the distance at which the evanescent wave intensity drops to I_0/e. It can be calculated as

$$d = \frac{\lambda}{4\pi\sqrt{(n_1^2 \sin^2(\theta) - n_2^2)}}$$

where λ is the incident light wavelength, n_1 is the refractive index of the higher–refractive index medium such as glass (1.518), and n_2 is the refractive index of the lower–refractive index medium such as water (1.33) or cell cytosol (1.33–1.37). Here θ is the incident angle that is larger than the so-called critical angle θ_c, the incident angle at which total internal reflection of the light occurs. The angle θ_c is related to only the refractive indices of n_1 and n_2 by

$$\sin(\theta_c) = \frac{n_2}{n_1}$$

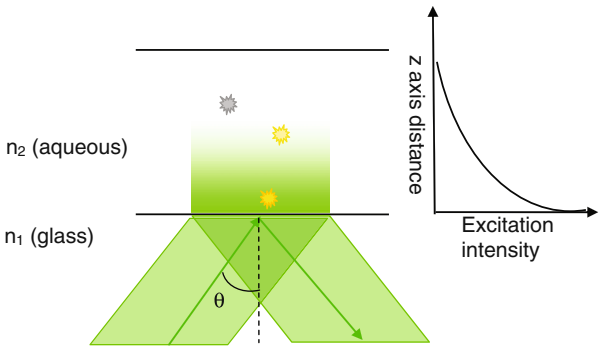

Figure 3.9. Schematic drawing of the concept of total internal reflection at the interface of glass and water. The laser beam passes through the glass and is reflected at the glass–water boundary at an angle larger than the critical angle θ_c, establishing an evanescent wave that penetrates into water in the sample chamber and decays exponentially along the z axis, therefore exciting only a few hundred nanometers from the interface.

Based on these equations, one can calculate that for a 514-nm excitation with an incident angle of 65°, the penetration depth d in cell cytosol is about 300 nm. Increasing the incident angle further decreases the penetration depth and allows only a thin layer above the coverslip to be effectively excited. Therefore, fluorescent molecules above the thin layer cannot be excited, and background is dramatically reduced. In addition, the illumination area of the incident laser beam can be adjusted to be as large as what is used in wide-field illumination, so that multiple molecules can be imaged simultaneously at a high frame rate. These properties render TIR illumination nearly the best choice for single-molecule imaging in live-cell imaging, although it limits observation to cellular events that occur close to the glass/cell interface. In addition, integrated fluorescent intensities of single molecules will have large variations, depending on their distances from the glass/cell interface; therefore care should be taken when determining whether a detected fluorescent spot is due to a single molecule or not.

There are two types of TIR illumination configurations, prism and objective type. In the prism-type configuration, cells are sandwiched between a glass slide and a coverslip, and the excitation laser beam is guided to the sample through a prism mounted on the top of the glass slide. The incident angle is adjusted by translating the beam relative to the prism. Fluorescence emitted by the sample is collected through the objective at the bottom of the coverslip. Because oil objectives with high numerical aperture are usually used to allow sensitive single-molecule detection, the thickness of the sample cannot exceed 15 μm, which often comprises the viability of cells during an extended period of imaging. Nevertheless, prism-type TIR has been successfully applied to imaging single GFP molecules in live fission yeast, *Dictyostelium discoideum*, and Jurkat cells [194].

The objective-type TIR is more suitable for live-cell imaging than the prism type. In this configuration, the excitation laser beam is focused to the periphery instead of the center of the back focal plane of the objective. Translating the beam in parallel to the center axis of the objective changes the incident angle of the light but not the position of illumination area. Tilting the beam relative to the center axis of the objective changes the incident angle as well, but the position of the illumination area is also changed; thus usually this configuration is not recommended. Because only an incident angle larger than the critical angle allows TIR illumination, and that maximal incident angle of the laser beam is limited by the numerical aperture (NA) of the objective, in that

$$\sin(\theta) = \frac{\mathrm{NA}}{n_3}$$

where θ is the maximal incident angle allowed by the objective and n_3 is the refractive index of the working medium (oil at 1.52, matching that of glass) of the objective, one can derive that NA needs to be greater than n_1, the refractive index of a cell (1.37), to achieve TIR illumination. Therefore, a high-NA objective, typically at 1.45, is essential in this type of configuration.

3.7.3. Camera-Based Detectors

Array detectors such as charged-coupled device (CCD) cameras instead of point detectors such as PMTs or APDs are usually used for single-molecule imaging in live cells. The selection criteria of those cameras are the same for single-molecule *in vitro* imaging. In

general these cameras are capable of single-photon detection and possess high quantum efficiency in converting photons into electrons, low readout noise, and a fast frame rate.

A CCD camera detects incoming photons on a two-dimensional array of tiny detector elements (or pixels) that are microns in size. When an incident photon hits one of the detector elements it has a probability of generating one electron from the element. This probability is the quantum efficiency of a CCD camera, and it can reach 0.95 in the newest generation of electron-multiplying (EM) CCD cameras. The electrons generated by the photons are then stored in the element until it is ready to be read out; charges are moved from each element of the array to an output register, and the contents of the output register are then amplified and read out. The speed to move the charges in each element and the output register limits the readout speed of the camera and hence the time resolution of an experiment.

Both intensified ICCD cameras and EM-CCDs have been used for single-molecule detection, but EM-CCDs possess clear advantages over ICCDs. EM-CCDs have high quantum efficiency (up to 0.95), while that of ICCDs is 0.2–0.5. In addition, EM-CCDs effectively minimize readout noise by amplifying the signal before readout noise is added by the output register; therefore, high frame rates of a few hundred hertz can be reached, and the readout noise is still negligible. By using small imaging area or binning pixels, one can further increase the frame rate but at the cost of decreased spatial resolution. A range of manufacturers such as Andor Technology, Hamamatsu, and Roper Scientific offer EM-CCDs that have quite comparable specifications for the key features such as quantum efficiency and pixel size but differ subtly in operating temperature, noise level, and so on. Therefore, the choice of which camera to use is dependent on personal preferences and specific applications.

3.7.4. Live-Cell Sample Preparation

A well-maintained cell chamber for optimal cell growth during a prolonged imaging period is essential for the success of experiments. In general, such a chamber has a coverslip at the bottom through which attached cells are imaged. Growth medium is added on top of cells, and the temperature of the chamber is maintained constantly. The detailed configuration of the chamber is dependent on the type of cells and the specific need of each experiment. The following paragraphs discuss the sample preparation for generic bacterial and mammalian cells.

For continuous growth of bacterial cells (or yeast cells) on the microscope stage, a sealed growth chamber is often used. The chamber can be homemade by spotting bacterial culture on top of a low–melting temperature agarose gel pad made with M9 growth medium, with the gel pad sandwiched between two coverslips separated by a spacer. The whole chamber is then sealed with glue to avoid dehydration over long periods of imaging. An objective heater can be employed to warm the chamber through the contact of the objective with the bottom coverslip of the chamber. Although this method is cost-effective and bacterial cells in the chamber can grow for multiple generations, the temperature of the chamber is not well regulated and often exhibits large fluctuations if the objective heater temperature is set much higher than the ambient room temperature. Therefore, this method is best suited for bacterial cell imaging at room temperature or when temperature fluctuations do not have significant impact on the cellular process of interest.

A commercially available cell growth chamber (Bioptechs, FCS2) has a similar geometry as the homemade chamber, but the temperature of the chamber can be accurately regulated through a specially designed glass slide at the top of the chamber. In addition, the FCS2 system allows the perfusion of growth media through the chamber, making it possible to study

the responses of cells to environmental stimulations. For a detailed description of how to use this chamber to monitor live bacterial cells, readers are referred to Xiao et al. [163] and the manufacturer's instructions.

The FCS2 system can also be used for mammalian cells. Cells are first cultured on coverslips immersed in growth media as usual, and then the coverslip is assembled into the closed chamber for observation. An open-dish format, in which the chamber is not sealed by the use of a top glass slide, is also popular in live-cell imaging. The easiest open-dish format is essentially a culture dish with a coverslip mounted at the bottom. This format allows easy addition of chemical stimuli but, again, suffers from unregulated temperature and media evaporation during long experiments. One important consideration for mammalian culture on a microscope stage is that if the medium is not perfused with CO_2 during the experiment, a growth medium with its pH not dependent on CO_2 such as Leibovitz's L15 should be used.

Besides these basic cell culture formats for live-cell imaging, many companies manufacture chambers with different geometries to meet specific needs and that address some of the concerns in the foregoing. Readers are referred to a collection of those companies (and other considerations for maintaining live cells on a microscope stage) at http://www.microscopyu.com/articles/livecellimaging/chamberresources.html. In addition, there is an excellent review describing the methods and considerations in live-cell imaging in much more detail [195].

The foregoing descriptions are for general live-cell imaging. To achieve single-molecule detection, however, there are some special considerations. The coverslip used in these growth chambers has to be thoroughly cleaned using cycles of ethanol, potassium hydroxide, and acetone [163]. This is to avoid dirt and background fluorescence from the coverslip. For this reason, commercially available culture dishes with a coverslip mounted at the bottom are not suitable for single-molecule imaging. If this format has to be used, it is recommended to manually mount cleaned coverslips to culture dishes with a hole drilled in the middle. In addition, defined, colorless growth medium needs to be used to minimize background fluorescence from the medium. It is also not recommended to use a large box to encapsulate the entire microscope and blow warm air into the box to maintain culture temperature. The air flow inside the box creates instability in the imaging systems, which is especially critical if sub–diffraction-limited resolution of single molecules is to be achieved. In addition, the temperature in those large boxes is usually not homogeneous, and a slight change of temperature even of 1°C could cause the optics in the microscope or box to move and cause focus or laser alignment drift.

3.8. Applications

In the last few years, single-molecule imaging in live cells have been employed to study gene expression [4,23,84], transcription factor–DNA interactions [196], cell signaling [31,33,197], protein complex composition [198–200], membrane protein dynamics [91,94,95,123,201–204], and cytoskeletal protein dynamics [92,96,159,205]. In addition, by amplifying the fluorescent signal by multifluorophore labeling or using a fluorogenic substrate, it has been possible to examine the dynamics in gene expression [4,10] and the movement of individual DNA and mRNA transcripts [3,5–8]. The following subsections discuss a few representative studies of single-molecule imaging in live cells. Studies in membrane and cytoskeletal protein dynamics share similar methods in that single-molecule tracking is used; they are discussed in Chapters 1 and 8and are not included here.

3.8.1. Gene Expression

Gene expression is inherently a stochastic process due to the small copy numbers of the participants such as DNAs, mRNAs, and transcription factors [11–13,206,207]. However, this stochasticity is often masked in ensemble studies and underestimated when overexpression of a gene has to be used to achieve detectable signal. If each single protein or mRNA molecule produced from a gene can be observed and counted in real time inside a live cell, the stochasticity of gene expression can be quantified and the molecular mechanisms of translation and transcription revealed.

To achieve this goal, Yu and Xiao et al. developed a single-molecule gene-expression reporter that allows the counting of protein molecules generated one at a time for multiple generations in live *E. coli* cells (Figure 3.10A) [84]. The reporter is generated by fusing a membrane-targeting sequence (MTS) to the YFP variant Venus. On expression, the reporter quickly folds and is targeted to the membrane so that its diffusion is slowed down. Therefore, the emitted photons of the reporter can be collected from a diffraction-limited spot, greatly enhancing the signal-to-background ratio. Using this reporter, the authors monitored the leaky expression of a repressed *lac* promoter, revealing that protein molecules are generated in randomly spaced bursts, corresponding to a Poissonian transcription process, and that the number of protein molecules generated from one mRNA molecule follows a geometric distribution due to the competition between RNaseE and ribosome binding of the mRNA molecule. This experiment is a good example of how a particular FP is selected to meet the particular experimental design—The FP needs to mature fast enough to report the production of a protein molecule as soon as it is generated and to be photoliable enough so that following its detection the FP can be photobleached quickly to avoid background accumulation.

In a different work by the same research group, the induction mechanism of the *lac* operon was investigated [23]. The authors found that in the presence of an inducer, a significant portion of the uninduced cells contain a few *lac* permease (LacY) molecules, disproving the long-held view in which a single LacY molecule, coupled with the positive feedback of the operon, is sufficient for induction [208]. Without the ability to visualize and count single permease molecules inside the cells, this conclusion would be difficult to reach. In addition, the authors monitored the real-time expression of *lac* permease using the same single-molecule gene expression reporter. They discovered that rare (once every many cell cycles) and large expression bursts of permease molecules (a few hundred), likely caused by the stochastic, complete dissociation of *lac* repressor from the operators, is the prerequisite for induction. This suggests a novel mechanism by which that an *E. coli* cell's decision to be induced or not hinges on the stochastic behavior of a single repressor molecule.

At the transcription level, Golding et al. used a MS2-GFP fusion protein to monitor the real-time production of single mRNA molecules that have 96 repeats of MS2 RNA-binding loops incorporated (Figure 3.10B) [4]. Under induced condition, Golding et al. found that mRNA molecules are produced in clustered bursts and are separated by periods of inactivity, corresponding to stochastic transitions of the promoter between active and inactive periods. This indicates that even in bacterial cells that lack a chromatin structure, there are other mechanisms that cause large fluctuations in transcription activity similar to those observed in eukaryotic cells [209,210].

3.8.2. Transcription Factor Dynamics

Single-molecule techniques can be used to address transient molecular interactions, especially for cellular components that exist at very low copy numbers. For example, the

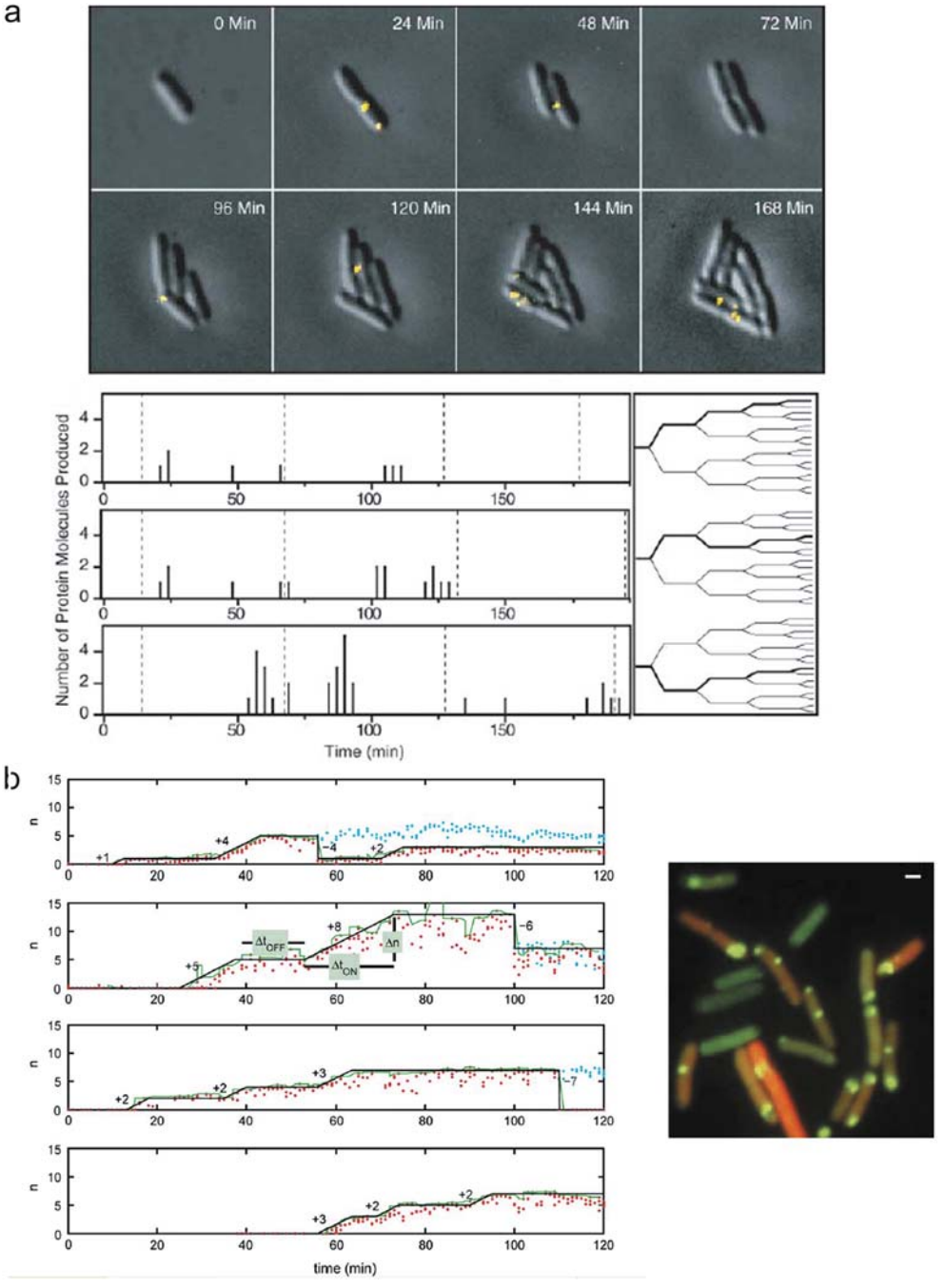

Figure 3.10. A. Single protein molecules counted in live *Escherichia coli* cells as they are generated one at a time [84]. **Top.** Sequences of an *E. coli* colony growing on a microscope stage with expressed single Tsr-Venus proteins shown in yellow. **Bottom.** Time traces of expressed Tsr-Venus molecules counted in real time. **B**. Single mRNA molecules counted in live *E. coli* cells [4]. *Left*: Time traces of mRNA production counted in real time. *Right*: Fluorescence image of *E. coli* cells expressing mRNA molecules tagged with a 96-ms^2 looped bound by MS2-GFP fusion proteins. Each green dot corresponds to one or a few mRNA molecules. (Figures reprinted with permission.)

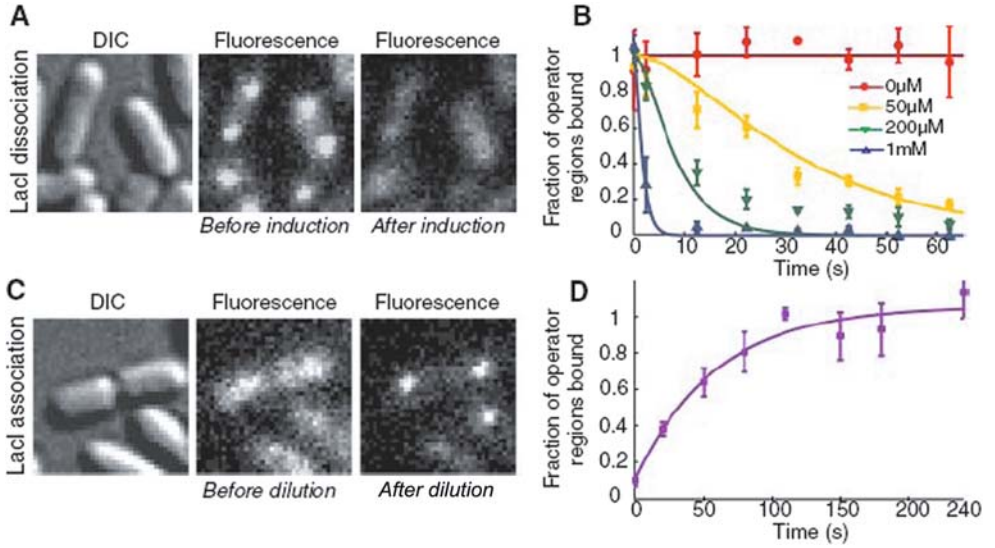

Figure 3.11. Imaging of *lac* repressor dynamics in live *Escherichia coli* cells [196]. **A.** *E. coli* cells before and 40 sec after addition of the inducer isopropyl-β-D-thiogalactopyranoside (IPTG). The disappearance of the bright fluorescent spot in the cells corresponds to the dissociation of LacI repressor from DNA. **B.** Fraction of *lac* operators that are LacI bound plotted as a function of time after induction by various concentrations of IPTG. **C.** *E. coli* cells before and 1 min after dilution of IPTG from 100 to 2 μM and with the addition of 1 mM of the IPTG-binding inhibitor orthonitrophenylfucoside (ONPF. **D.** Fraction of the operators that are LacI-bound as a function of time after rapid dilution of IPTG from 100 to 2 nM. (Figures reprinted with permission.)

binding of transcription factors to their corresponding DNA sitesplays an important role in regulating gene expression and has been subject to intensive genetic, biochemical, and biophysical studies, but the direct observation of the specific and nonspecific DNA binding of a single transcription factor inside live *E. coli* cells has just become possible (Figure 3.11) [196]. Using a LacI-Venus fusion, Elf et al. [196] monitored the binding of a single *lac* repressor LacI to its operator site *lacO* in response to the inducer isopropyl-β-D-thiogalactopyranoside (IPTG) in live *E. coli* cells. In the absence of IPTG, the repressor bound tightly to *lacO* and was detected as a diffraction-limited spot. When IPTG was added, the clear fluorescent spot disappeared within seconds, indicating the quick dissociation of the repressor from the operator site. If IPTG was removed subsequently, the fluorescent spot reappeared within 1 min. From this it was calculated that it takes one repressor molecule up to ∼360 sec to find a *lac*O site inside the cell. During the 360 sec, the repressor spends 90% of its time to diffuse one-dimensionally on nonspecific DNA for up to 5 ms before it hops to another DNA segment to start a new round of searching again. This is the first quantitative demonstration of the search of a transcription factor for its binding site in live cells. This would be impossible without the ability to image single molecules inside live cells.

Similarly, the binding of Venus-tagged T7 RNA polymerase (RNAP) molecules on an engineered T7 promoter was observed in live *E. coli* cells [116]. The T7 promoter is controlled by the *lac* repressor and integrated on the *E. coli* chromosome. After addition of IPTG, multiple T7 RNAP molecules were found to bind to the promoter region, indicating multiple active transcription processes. This is exciting, in that it allows direct observation of the promoter

state, which could possibly provide a mechanism for the transcription bursts observed previously [4,23].

3.8.3. Cell Signaling

Cellsrespond to environmental cues through vast signal transduction networks. Using single-molecule techniques, it is possible to directly observe the signal flow in this process and the dynamics of molecular interactions in real time. Sako et al. labeled the epidermal growth factor (EGF) with Cy3 and found that Cy3-EGF binds to the receptor (EGFR) within a few seconds after its addition into the culture medium [31]. Of interest, during this process, they observed that the fluorescence intensity of one spot, corresponding to one bound Cy3-EGF molecule, suddenly increased twofold, indicating the binding of another CY3-EGF molecule (Figure 3.12). This suggests that the dimerization of EGFR, a prerequisite for the downstream Ca^{2+} response, occurs at least before the binding of the second EGF molecule. In addition, the binding of the second Cy3-EGF to an EGF-bound EGFR dimer in the presence of a high concentration of unbound EGFR monomers (or dimers) indicates that the binding of the first EGF may enhance the binding of the second EGF through a cooperative mechanism.

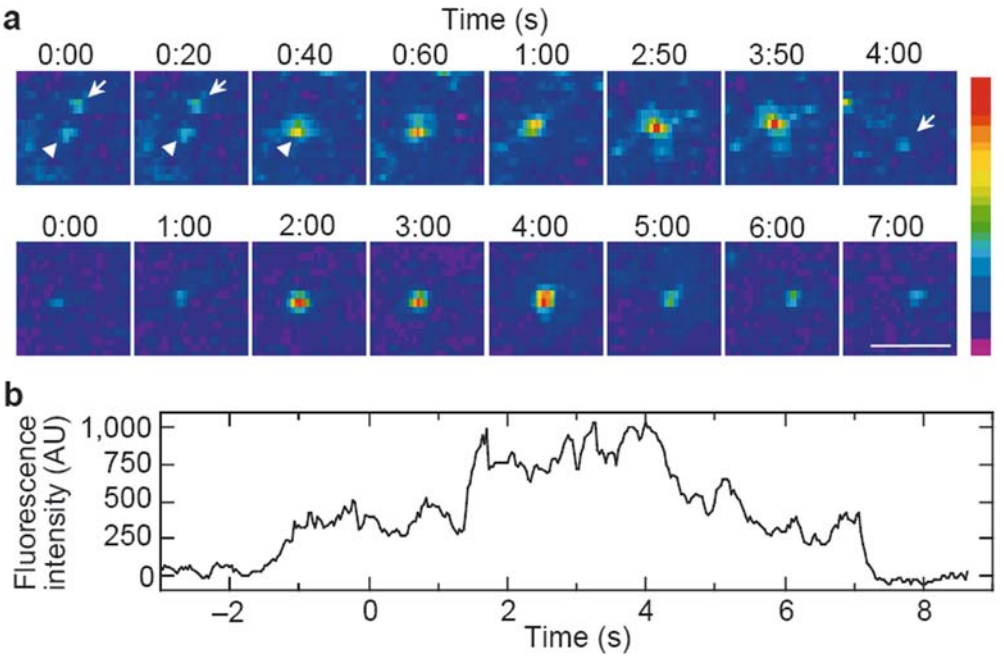

Figure 3.12. Imaging of the dimerization of epidermal growth factor (EGF)–EGF receptor complexes at the single-molecule level [31]. **A.** In the upper panel, two spots (*arrow and arrowhead*) collided at time 0:40 sec and then moved together. The fluorescence intensity increased after the collision. At 4:00 sec, the intensity of the spot decreased to about half (*arrow*), probably because of photobleaching of one Cy3-EGF molecule. In the second panel, a fluorescence spot with the intensity of a single molecule was observed until 1:00 sec; the intensity of the spot increased suddenly between 1:00 and 2:00 sec, then decreased between 4:00 and 5:00 sec. The scale bar represents 5 mm. **B.** Time trace of the fluorescence intensity of the spot shown in the second panel of panel A. A two-step increase and bleaching of the intensity can be seen. The time trace is noisy because of slow, lateral diffusive movement of the spot. (Figures reprinted with permission.)

Conformational fluctuations between the two monomers within one EGFR dimer were also observed by labeling one monomer with Cy3 and the other with Cy5 and monitoring the FRET signal between the pair.

Another study monitored the interaction of the small G protein Ras with its cofactor GTP in live cells using single-molecule FRET (sm-FRET) [33]. In this work, Ras is expressed as a fusion protein to YFP, and the dye-conjugated Bodipy-GTP is microinjected into the cell. On stimulation by the addition of EGF, within 1 min, YFP-Ras molecules became stationary, BodipyTR-GTP molecules appeared as a clear spot on the membrane at exactly the positions of YFP-Ras molecules, and FRET between YFP and Bodipy was observed. However, the BodipyTR dye is not photostable enough to allow the imaging of its turnover by Ras, which would be interesting to correlate with the recruitment of downstream proteins in the signal transduction pathway. This highlights the importance of developing new photostable dyes to allow such applications.

In both studies, sm-FRET was used to observe the protein–protein or protein–ligand interactions. Organic dyes were used as the FRET acceptor not only because the molecules they labeled are small molecules, but also because their spectral properties are better suited for sm-FRET in live cells than are those of available RFPs. This limits the use of sm-FRET in bacterial cells because dye-labeled ligand or proteins cannot be introduced into cells by microinjection. In addition, in eukaryotic cells some ligands or proteins of interest may be hard to modify to incorporate the dye. There is no report of live-cell sm-FRET based on two FPs, possibly due to the fact that current RFPs can also be directly excited around 488 nm, the wavelength that excites the potential donor GFP. CFP and YFP have been proven to be a good FRET pair at the ensemble level [79], but CFP is not detectable at the single-molecule level due to the high autofluorescence background in that wavelength range [76]. Developing a bright far-red FP to pair with GFP or YFP will significantly enhance current research capacity for probing protein–protein interactions in live cells at the single-molecule level.

3.8.4. Protein Complex Composition

In addition to monitoring gene expression and molecular interactions, the multimeric state and composition of a protein complex in live cells can be measured using single-molecule imaging. Ulbrich and Isacoff reported a single-molecule assay to count the copy numbers of subunits of proteins in live cell membranes by taking advantage of the discrete steps of photobleaching of single molecules [200]. This method was used to determine the numbers of subunits NR1 and NR3 in the glutamate-gated receptor *N*-methyl-D-aspartate (NMDA) [211]. In another study, the copy numbers of seven kinetochore proteins tagged with GFP in budding yeast were determined, not by discrete photobleaching, but by the integrated fluorescence intensity normalized against the known single-GFP-molecule intensity [212]. The limitation of these methods is that the copy numbers cannot exceed more than a few molecules per spot because the higher the copy number, the more likely it is that two molecules are photobleached at the same time and the greater is the error in using integrated intensity to determine the total copy number of molecules due to the stochastic nature of photobleaching.

Recent advances in single-molecule superresolution imaging have enabled the application of these highly promising techniques in live cells [123,137,158,213]. These techniques not only allow the quantification of the composition of a protein complex, but also provide nanometer resolution of the spatial organization of the complex. Their potentials cannot be

underestimated. Because they are discussed in detail in Chapter 10, they are not included here, and readers are encouraged to see the related information and references there.

3.9. Outlook

Recent advances in single-molecule imaging techniques and FP development have enabled the direct visualization of cellular processes and molecular interactions as they occur in real time inside live cells. This opens a wide window for investigating many fundamental biological questions at a level that was inaccessible by population studies before. Yet this field is still young. Development of better FPs and more powerful imaging techniques, such as spectrally separable FP pairs for sm-FRET imaging in live cells, fast-maturing FPs for correlating the expression of multiple genes, and multicolor superresolution imaging in live cells, promises to bring in even more exciting discoveries. With the continuing efforts in pushing current technical limits, in the near future it may no longer be a fantasy for a biologist to directly visualize the dynamics of individual molecules in multiplex with high temporal and spatial resolution in various live cells, tissues, and even animals, discovering unprecedented molecular details at a systems level.

References

1. Moerner, W. E., and L. Kador (1989). Optical detection and spectroscopy of single molecules in a solid. Phys Rev Lett, **62**(21): 2535–8.
2. Orrit, M., and J. Bernard (1990). Single pentacene molecules detected by fluorescence excitation in a *p*-terphenyl crystal. Phys Rev Lett, **65**(21): 2716–19.
3. Shav-Tal, Y., X. Darzacq, et al. (2004). Dynamics of single mRNPs in nuclei of living cells. Science, **304**(5678): 1797–800.
4. Golding, I., J. Paulsson, et al. (2005). Real-time kinetics of gene activity in individual bacteria. Cell, **123**(6): 1025–36.
5. Fusco, D., N. Accornero, et al. (2003). Single mRNA molecules demonstrate probabilistic movement in living mammalian cells. Curr Biol, **13**(2): 161–7.
6. Bates, D., and N. Kleckner (2005). Chromosome and replisome dynamics in E. coli: loss of sister cohesion triggers global chromosome movement and mediates chromosome segregation. Cell, **121**(6): 899–911.
7. Lemon, K. P., and A. D. Grossman (2000). Movement of replicating DNA through a stationary replisome. Mol Cell, **6**(6): 1321–30.
8. Viollier, P. H., M. Thanbichler, et al. (2004). Rapid and sequential movement of individual chromosomal loci to specific subcellular locations during bacterial DNA replication. Proc Natl Acad Sci USA, **101**(25): 9257–62.
9. Rotman, B. (1961). Measurement of activity of single molecules of beta-D-galactosidase. Proc Natl Acad Sci USA, **47**: 1981–91.
10. Cai, L., N. Friedman, and X. S. Xie (2006). Stochastic protein expression in individual cells at the single molecule level. Nature, **440**(7082): 358–62.
11. Ghaemmaghami, S., W. K. Huh, et al. (2003). Global analysis of protein expression in yeast. Nature, **425**(6959): 737–41.
12. Guptasarma, P. (1995). Does replication-induced transcription regulate synthesis of the myriad low copy number proteins of Escherichia *coli*? Bioessays, **17**(11): 987–97.
13. Freund, J. A., and T. Poschel (2005). *Stochastic Processes in Physics, Chemistry, and Biology*. Springer: Berlin.
14. Elowitz, M. B., A. J. Levine, et al. (2002). Stochastic gene expression in a single cell. Science, **297**(5584): 1183–6.
15. Ozbudak, E. M., M. Thattai, et al. (2002). Regulation of noise in the expression of a single gene. Nat Genet, **31**(1): 69–73.

16. Weinberger, L. S., J. C. Burnett, et al. (2005). Stochastic gene expression in a lentiviral positive-feedback loop: HIV-1 Tat fluctuations drive phenotypic diversity. Cell, **122**(2): 169–82.
17. Huang, C. Y., and J. E. Ferrell, Jr. (1996). Ultrasensitivity in the mitogen-activated protein kinase cascade. Proc Natl Acad Sci USA, **93**(19): 10078–83.
18. Braun, H. A., H. Wissing, et al. (1994). Oscillation and noise determine signal transduction in shark multimodal sensory cells. Nature, **367**(6460): 270–3.
19. Wang, W., and Z. D. Wang (1997). Internal-noise-enhanced signal transduction in neuronal systems. Phys Rev E, **55**(6): 7379–84.
20. Bezrukov, S. M., and I. Vodyanoy (1995). Noise-induced enhancement of signal transduction across voltage-dependent ion channels. Nature, **378**(6555): 362–4.
21. Arkin, A., J. Ross, and H. H. McAdams (1998). Stochastic kinetic analysis of developmental pathway bifurcation in phage lambda-infected *Escherichia coli* cells. Genetics, **149**(4): 1633–48.
22. Suel, G. M., J. Garcia-Ojalvo, et al. (2006). An excitable gene regulatory circuit induces transient cellular differentiation. Nature, **440**(7083): 545–50.
23. Choi, P. J., L. Cai, et al. (2008). A stochastic single-molecule event triggers phenotype switching of a bacterial cell. Science, **322**(5900): 442–6.
24. Maamar, H., A. Raj, and D. Dubnau (2007). Noise in gene expression determines cell fate in *Bacillus subtilis.* Science, **317**(5837): 526–9.
25. Kussell, E., R. Kishony, et al. (2005). Bacterial persistence: a model of survival in changing environments. Genetics, **169**(4): 1807–14.
26. Berland, K. M., P. T. So, and E. Gratton (1995). Two-photon fluorescence correlation spectroscopy: method and application to the intracellular environment. Biophys J, **68**(2): 694–701.
27. Brock, R., M. A. Hink, and T. M. Jovin (1998). Fluorescence correlation microscopy of cells in the presence of autofluorescence. Biophys J, **75**(5): 2547–57.
28. Schwille, P., U. Haupts, et al. (1999). Molecular dynamics in living cells observed by fluorescence correlation spectroscopy with one- and two-photon excitation. Biophys J, **77**(4): 2251–65.
29. Komarova, Y., J. Peloquin, and G. Borisy (2005). Microinjection of fluorophore-labeled proteins. In *Live Cell Imaging, a Laboratory Manual*, R. D. Goldman and D. L. Spector, Editors. Cold Spring Harbor Laboratory Press: Cold Spring Harbor, New York, pp. 67–86.
30. O'Hare, H. M., K. Johnsson, and A. Gautier (2007). Chemical probes shed light on protein function. Curr Opin Struct Biol, **17**(4): 488–94.
31. Sako, Y., S. Minoghchi, and T. Yanagida (2000). Single-molecule imaging of EGFR signalling on the surface of living cells. Nat Cell Biol, **2**(3): 168–72.
32. Schütz, G. J., G. Kada, et al. (2000). Properties of lipid microdomains in a muscle cell membrane visualized by single molecule microscopy. EMBO J **19**: 892–901.
33. Murakoshi, H., R. Iino, et al. (2004). Single-molecule imaging analysis of Ras activation in living cells. Proc Natl Acad Sci USA, **101**(19): 7317–22.
34. Guignet, E. G., J. M. Segura, et al. (2007). Repetitive reversible labeling of proteins at polyhistidine sequences for single-molecule imaging in live cells. Chemphyschem, **8**(8): 1221–7.
35. Lord, S. J., N. R. Conley, et al. (2008). A photoactivatable push-pull fluorophore for single-molecule imaging in live cells. J Am Chem Soc. (2008) Jul 23; **130**(29): 9204–5.
36. Lord, S. J., Z. Lu, et al. (2007). Photophysical properties of acene DCDHF fluorophores: long-wavelength single-molecule emitters designed for cellular imaging. J Phys Chem A, **111**(37): 8934–41.
37. Michalet, X., F. F. Pinaud, et al. (2005). Quantum dots for live cells, *in vivo* imaging, and diagnostics. Science, **307**(5709): 538–44.
38. Zhou, M., and I. Ghosh (2007). Quantum dots and peptides: a bright future together. Biopolymers, **88**(3): 325–39.
39. Davenport, D., and J. A. C. Nicol (1955). Luminescence of Hydromedusae. Proc R Soc B, **144**: 399–411.
40. Shimomura, O., F. H. Johnson, and Y. Saiga (1962). Extraction, purification and properties of aequorin, a bioluminescent protein from the luminous hydromedusan, *Aequorea.* J Cell Comp Physiol, **59**: 223–39.
41. Hastings, J. W., and J. G. Morin (1969). Comparative biochemistry of calcium photoproteins from the ctenophore, *Mnemiopsis* and the coelenterates *Aequorea*, *Obelia*, *Pelagia* and *Renilla.* Biol Bull, **137**: 402.
42. Morin, J. G., and J. W. Hastings (1971). Energy transfer in a bioluminescent system. J Cell Physiol, **77**(3): 313–8.
43. Morise, H., O. Shimomura, et al. (1974). Intermolecular energy transfer in the bioluminescent system of *Aequorea.* Biochemistry, **13**(12): 2656–62.

44. Mills, C. E. (2001). Jellyfish blooms: are populations increasing globally in response to changing ocean conditions? Hydrobiologia, **451**: 55–68.
45. Prasher, D. C., V. K. Eckenrode, et al. (1992). Primary structure of the *Aequorea victoria* green-fluorescent protein. Gene, **111**(2): 229–33.
46. Chalfie, M., Y. Tu, et al. (1994). Green fluorescent protein as a marker for gene expression. Science, **263**(5148): 802–5.
47. Heim, R., D. C. Prasher, and R. Y. Tsien (1994). Wavelength mutations and posttranslational autoxidation of green fluorescent protein. Proc Natl Acad Sci USA, **91**(26): 12501–4.
48. Inouye, S., and F. I. Tsuji (1994). *Aequorea* green fluorescent protein. Expression of the gene and fluorescence characteristics of the recombinant protein. FEBS Lett, **341**(2–3): 277–80.
49. Heim, R., A. B. Cubitt, and R. Y. Tsien (1995). Improved green fluorescence. Nature, **373**(6516): 663–4.
50. Yang, F., L. G. Moss, and G. N. Phillips, Jr. (1996). The molecular structure of green fluorescent protein. Nat Biotechnol, **14**(10): 1246–51.
51. Ormo, M., A. B. Cubitt, et al. (1996). Crystal structure of the *Aequorea victoria* green fluorescent protein. Science, **273**(5280): 1392–5.
52. Cubitt, A. B., F. Carrel, et al. (1992). Molecular genetic analysis of signal transduction pathways controlling multicellular development in *Dictyostelium.* Cold Spring Harb Symp Quant Biol, **57**: 177–92.
53. Reid, B. G., and G. C. Flynn (1997). Chromophore formation in green fluorescent protein. Biochemistry, **36**(22): 6786–91.
54. Rosenow, M. A., H. A. Huffman, et al. (2004). The crystal structure of the Y66L variant of green fluorescent protein supports a cyclization-oxidation-dehydration mechanism for chromophore maturation. Biochemistry, **43**(15): 4464–72.
55. Rosenow, M. A., H. N. Patel, and R. M. Wachter (2005). Oxidative chemistry in the GFP active site leads to covalent cross-linking of a modified leucine side chain with a histidine imidazole: implications for the mechanism of chromophore formation. Biochemistry, **44**(23): 8303–11.
56. Zhang, L., H. N. Patel, et al. (2006). Reaction progress of chromophore biogenesis in green fluorescent protein. J Am Chem Soc, **128**(14): 4766–72.
57. Barondeau, D. P., C. J. Kassmann, et al. (2005). Understanding GFP chromophore biosynthesis: controlling backbone cyclization and modifying post-translational chemistry. Biochemistry, **44**(6): 1960–70.
58. Ward, W. W., H. J. Prentice, et al. (1982). Spectral perturbations of the *Aequorea* green fluorescent protein. Photochem Photobiol, **35**: 803–8.
59. Voityuk, A. A., A. D. Kummer, et al. (2001). Absorption spectra of the GFP chromophore in solution: comparison of theoretical and experimental results. Chem Phys, **269**(1–3): 83–91.
60. Chattoraj, M., B. A. King, et al. (1996). Ultra-fast excited state dynamics in green fluorescent protein: multiple states and proton transfer. Proc Natl Acad Sci USA, **93**(16): 8362–7.
61. van Thor, J. J., T. Gensch, et al. (2002). Phototransformation of green fluorescent protein with UV and visible light leads to decarboxylation of glutamate 222. Nat Struct Biol, **9**(1): 37–41.
62. Cubitt, A. B., R. Heim, et al. (1995). Understanding, improving and using green fluorescent proteins. Trends Biochem Sci, **20**(11): 448–55.
63. Cubitt, A. B., L. A. Woollenweber, and R. Heim (1999). Understanding structure–function relationships in the *Aequorea victoria* green fluorescent protein. Methods Cell Biol, **58**: 19–30.
64. Remington, S. J. (2006). Fluorescent proteins: maturation, photochemistry and photophysics. Curr Opin Struct Biol, **16**(6): 714–21.
65. McAnaney, T. B., W. Zeng, et al. (2005). Protonation, photobleaching, and photoactivation of yellow fluorescent protein (YFP 10C): a unifying mechanism. Biochemistry, **44**(14): 5510–24.
66. Shaner, N. C., M. Z. Lin, et al. (2008). Improving the photostability of bright monomeric orange and red fluorescent proteins. Nat Methods, **5**(6): 545–51.
67. Swaminathan, R., C. P. Hoang, and A. S. Verkman (1997). Photobleaching recovery and anisotropy decay of green fluorescent protein GFP-S65T in solution and cells: cytoplasmic viscosity probed by green fluorescent protein translational and rotational diffusion. Biophys J, **72**(4): 1900–7.
68. Peterman, E. J. G., S. Brasselet, and W. E. Moerner (1999). The fluorescence dynamics of single molecules of green fluorescent protein. J Phys Chem A, **103**(49): 10553–60.
69. Pierce, D. W., N. Hom-Booher, and R. D. Vale (1997). Imaging individual green fluorescent proteins. Nature, **388**(6640): 338.
70. Greenbaum, L., C. Rothmann, et al. (2000). Green fluorescent protein photobleaching: a model for protein damage by endogenous and exogenous singlet oxygen. Biol Chem, **381**(12): 1251–58.

71. Bulina, M. E., D. M. Chudakov, et al. (2006). A genetically encoded photosensitizer. Nat Biotechnol, **24**(1): 95–9.
72. Lakowicz, J. (2006). *Principles of Fluorescence Spectroscopy*, 3rd ed. Springer: New York.
73. Heikal, A. A., S. T. Hess, et al. (2000). Molecular spectroscopy and dynamics of intrinsically fluorescent proteins: coral red (dsRed) and yellow (Citrine). Proc Natl Acad Sci USA, **97**(22): 11996–2001.
74. Garcia-Parajo, M. F., G.M. Segers-Nolten, et al. (2000). Real-time light-driven dynamics of the fluorescence emission in single green fluorescent protein molecules. Proc Natl Acad Sci USA, **97**(13): 7237–42.
75. Shaner, N. C., P. A. Steinbach, and R. Y. Tsien (2005). A guide to choosing fluorescent proteins. Nat Methods, **2**(12): 905–9.
76. Harms, G. S., L. Cognet, et al. (2001). Autofluorescent proteins in single-molecule research: applications to live cell imaging microscopy. Biophys J, **80**(5): 2396–408.
77. Dickson, R. M., A. B. Cubitt, et al. (1997). On/off blinking and switching behaviour of single molecules of green fluorescent protein. Nature, **388**(6640): 355–8.
78. Moerner, W. E., E. J. Peterman, et al. (1999). Optical methods for exploring dynamics of single copies of green fluorescent protein. Cytometry, **36**(3): 232–8.
79. Miyawaki, A., and R. Y. Tsien (2000). Monitoring protein conformations and interactions by fluorescence resonance energy transfer between mutants of green fluorescent protein. Methods Enzymol, **327**: 472–500.
80. Nifosi, R., A. Ferrari, et al. (2003). Photoreversible dark state in a tristable green fluorescent protein variant. J Phys Chem B, **107**(7): 1679–84.
81. Haupts, U., S. Maiti, et al. (1998). Dynamics of fluorescence fluctuations in green fluorescent protein observed by fluorescence correlation spectroscopy. Proc Natl Acad Sci USA, **95**(23): 13573.
82. Evdokimov, A. G., M. E. Pokross, et al. (2006). Structural basis for the fast maturation of Arthropoda green fluorescent protein. EMBO Rep, **7**(10): 1006–12.
83. Nagai, T., K. Ibata, et al. (2002). A variant of yellow fluorescent protein with fast and efficient maturation for cell-biological applications. Nat Biotechnol, **20**(1): 87–90.
84. Yu, J., J. Xiao, et al. (2006). Probing gene expression in live cells, one protein molecule at a time. Science, **311**(5767): 1600–3.
85. Shaner, N. C., R. E. Campbell, et al. (2004). Improved monomeric red, orange and yellow fluorescent proteins derived from *Discosoma* sp. red fluorescent protein. Nat Biotechnol, **22**(12): 1567–72.
86. Tsien, R. Y. (1998). The green fluorescent protein. Annu Rev Biochem, **67**: 509–44.
87. Kennis, J. T., D. S. Larsen, et al. (2004). Uncovering the hidden ground state of green fluorescent protein. Proc Natl Acad Sci USA, **101**(52): 17988–93.
88. Cormack, B. P., G. Bertram, et al. (1997). Yeast-enhanced green fluorescent protein (yEGFP)a reporter of gene expression in *Candida albicans.* Microbiology, **143**(Pt 2): 303–11.
89. Brejc, K., T. K. Sixma, et al. (1997). Structural basis for dual excitation and photoisomerization of the *Aequorea victoria* green fluorescent protein. Proc Natl Acad Sci USA, **94**(6): 2306–11.
90. Wachter, R. M., D. Yarbrough, et al. (2000). Crystallographic and energetic analysis of binding of selected anions to the yellow variants of green fluorescent protein. J Mol Biol, **301**(1): 157–71.
91. Iino, R., I. Koyama, and A. Kusumi (2001). Single molecule imaging of green fluorescent proteins in living cells: E-cadherin forms oligomers on the free cell surface. Biophys J, **80**(6): 2667–77.
92. Watanabe, N., and T. J. Mitchison (2002). Single-molecule speckle analysis of actin filament turnover in Lamellipodia. Science, **295**(5557): 1083–6.
93. Pedelacq, J. D., S. Cabantous, et al. (2006). Engineering and characterization of a superfolder green fluorescent protein. Nat Biotechnol, **24**(1): 79–88.
94. Deich, J., E. M. Judd, et al. (2004). Visualization of the movement of single histidine kinase molecules in live *Caulobacter* cells. Proc Natl Acad Sci USA, **101**(45): 15921–6.
95. Harms, G. S., L. Cognet, et al. (2001). Single-molecule imaging of l-type Ca(2+) channels in live cells. Biophys J, **81**(5): 2639–46.
96. Kim, S. Y., Z. Gitai, et al. (2006). Single molecules of the bacterial actin MreB undergo directed treadmilling motion in *Caulobacter crescentus.* Proc Natl Acad Sci USA, **103**(29): 10929–34.
97. Chesler, M., and K. Kaila (1992). Modulation of pH by neuronal activity. Trends Neurosci, **15**(10): 396–402.
98. Mansoura, M. K., J. Biwersi, et al. (1999). Fluorescent chloride indicators to assess the efficacy of CFTR cDNA delivery. Hum Gene Ther, **10**(6): 861–75.
99. Zacharias, D. A., J. D. Violin, et al. (2002). Partitioning of lipid-modified monomeric GFPs into membrane microdomains of live cells. Science, **296**(5569): 913–6.
100. Griesbeck, O., G. S. Baird, et al. (2001). Reducing the environmental sensitivity of yellow fluorescent protein. Mechanism and applications. J Biol Chem, **276**(31): 29188–94.

101. Shaner, N. C., G. H. Patterson, and M. W. Davidson (2007). Advances in fluorescent protein technology. J Cell Sci, **120**(Pt 24): 4247–60.
102. Rekas, A., J. R. Alattia, et al. (2002). Crystal structure of Venus, a yellow fluorescent protein with improved maturation and reduced environmental sensitivity. J Biol Chem, **277**(52): 50573–8.
103. Nguyen, A. W., and P. S. Daugherty (2005). Evolutionary optimization of fluorescent proteins for intracellular FRET. Nat Biotechnol, **23**(3): 355–60.
104. Ohashi, T., S. D. Galiacy, et al. (2007). An experimental study of GFP-based FRET, with application to intrinsically unstructured proteins. Protein Sci, **16**(7): 1429–38.
105. Vinkenborg, J. L., T. H. Evers, et al. (2007). Enhanced sensitivity of FRET-based protease sensors by redesign of the GFP dimerization interface. Chembiochem, **8**(10): 1119–21.
106. Mishin, A. S., F. V. Subach, et al. (2008). The first mutant of the *Aequorea victoria* green fluorescent protein that forms a red chromophore. Biochemistry, **47**(16): 4666–73.
107. Elowitz, M. B., M. G. Surette, et al. (1997). Photoactivation turns green fluorescent protein red. Curr Biol, **7**(10): 809–12.
108. Sawin, K. E., and P. Nurse (1997). Photoactivation of green fluorescent protein. Curr Biol, **7**(10): R606–7.
109. Matz, M. V., A. F. Fradkov, et al. (1999). Fluorescent proteins from nonbioluminescent *Anthozoa* species. Nat Biotechnol, **17**(10): 969–73.
110. Baird, G. S., D. A. Zacharias, and R. Y. Tsien (2000). Biochemistry, mutagenesis, and oligomerization of DsRed, a red fluorescent protein from coral. Proc Natl Acad Sci USA, **97**(22): 11984–9.
111. Gross, L. A., G. S. Baird, et al. (2000). The structure of the chromophore within DsRed, a red fluorescent protein from coral. Proc Natl Acad Sci USA, **97**(22): 11990–5.
112. Wall, M. A., M. Socolich, and R. Ranganathan (2000). The structural basis for red fluorescence in the tetrameric GFP homolog DsRed. Nat Struct Biol, **7**(12): 1133–8.
113. Yarbrough, D., R. M. Wachter, et al. (2001). Refined crystal structure of DsRed, a red fluorescent protein from coral, at 2.0-A resolution. Proc Natl Acad Sci USA, **98**(2): 462–7.
114. Tubbs, J. L., J. A. Tainer, and E. D. Getzoff (2005). Crystallographic structures of Discosoma red fluorescent protein with immature and mature chromophores: linking peptide bond trans-cis isomerization and acylimine formation in chromophore maturation. Biochemistry, **44**(29): 9833–40.
115. Shu, X., K. Kallio, et al. (2007). Ultrafast excited-state dynamics in the green fluorescent protein variant S65T/H148D. 1. Mutagenesis and structural studies. Biochemistry, **46**(43): 12005–13.
116. Xie, X. S., P. J. Choi, et al. (2008). Single-molecule approach to molecular biology in living bacterial cells. Annu Rev Biophys, **37**: 417–44.
117. Karasawa, S., T. Araki, et al. (2004). Cyan-emitting and orange-emitting fluorescent proteins as a donor/acceptor pair for fluorescence resonance energy transfer. Biochem J, **381**(Pt 1): 307–12.
118. Shu, X., N. C. Shaner, et al. (2006). Novel chromophores and buried charges control color in mFruits. Biochemistry, **45**(32): 9639–47.
119. Vavylonis, D., J. Q. Wu, et al. (2008). Assembly mechanism of the contractile ring for cytokinesis by fission yeast. Science, **319**(5859): 97–100.
120. Merzlyak, E. M., J. Goedhart, et al. (2007). Bright monomeric red fluorescent protein with an extended fluorescence lifetime. Nat Methods, **4**(7): 555–7.
121. Petersen, J., P. G. Wilmann, et al. (2003). The 2.0-A crystal structure of eqFP611, a far red fluorescent protein from the sea anemone *Entacmaea quadricolor.* J Biol Chem, **278**(45): 44626–31.
122. Shcherbo, D., E. M. Merzlyak, et al. (2007). Bright far-red fluorescent protein for whole-body imaging. Nat Methods, **4**(9): 741–6.
123. Manley, S., J. M. Gillette, et al. (2008). High-density mapping of single-molecule trajectories with photoactivated localization microscopy. Nat Methods. 2008 Feb; **5**(2): 155–7.
124. Niu, L., and J. Yu (2008). Investigating intracellular dynamics of FtsZ cytoskeleton with photoactivation single-molecule tracking. Biophys J, **95**(4): 2009–16.
125. Verkhusha, V. V., and A. Sorkin (2005). Conversion of the monomeric red fluorescent protein into a photoactivatable probe. Chem Biol, **12**(3): 279–85.
126. Lukyanov, K. A., A. F. Fradkov, et al. (2000). Natural animal coloration can Be determined by a nonfluorescent green fluorescent protein homolog. J Biol Chem, **275**(34): 25879–82.
127. Ando, R., H. Mizuno, and A. Miyawaki (2004). Regulated fast nucleocytoplasmic shuttling observed by reversible protein highlighting. Science, **306**(5700): 1370–3.
128. Ando, R., H. Hama, et al. (2002). An optical marker based on the UV-induced green-to-red photoconversion of a fluorescent protein. Proc Natl Acad Sci USA, **99**(20): 12651–6.

129. Tsutsui, H., S. Karasawa, et al. (2005). Semi-rational engineering of a coral fluorescent protein into an efficient highlighter. EMBO Rep, **6**(3): 233–8.
130. Wiedenmann, J., S. Ivanchenko, et al. (2004). EosFP, a fluorescent marker protein with UV-inducible green-to-red fluorescence conversion. Proc Natl Acad Sci USA, **101**(45): 15905–10.
131. Gurskaya, N. G., V. V. Verkhusha, et al. (2006). Engineering of a monomeric green-to-red photoactivatable fluorescent protein induced by blue light. Nat Biotechnol, **24**(4): 461–5.
132. Chudakov, D. M., V. V. Verkhusha, et al. (2004). Photoswitchable cyan fluorescent protein for protein tracking. Nat Biotechnol, **22**(11): 1435–9.
133. Lukyanov, K. A., D. M. Chudakov, et al. (2005). Innovation: Photoactivatable fluorescent proteins. Nat Rev Mol Cell Biol, **6**(11): 885–91.
134. Patterson, G. H. (2008). Photoactivation and imaging of photoactivatable fluorescent proteins. Curr Protoc Cell Biol, **2008**(March): Chapter 21: Unit 21.6.
135. Lippincott-Schwartz, J., and G. H. Patterson (2008). Fluorescent proteins for photoactivation experiments. Methods Cell Biol, **85**: 45–61.
136. Cinelli, R. A., V. Tozzini, et al. (2001). Coherent dynamics of photoexcited green fluorescent proteins. Phys Rev Lett, **86**(15): 3439–42.
137. Biteen, J. S., M. A. Thompson, et al. (2008). Super-resolution imaging in live *Caulobacter crescentus* cells using photoswitchable EYFP. Nat Methods, **5**(11): 947–9.
138. Habuchi, S., R. Ando, et al. (2005). Reversible single-molecule photoswitching in the GFP-like fluorescent protein Dronpa. Proc Natl Acad Sci USA, **102**(27): 9511–6.
139. Andresen, M., A. C. Stiel, et al. (2007). Structural basis for reversible photoswitching in Dronpa. Proc Natl Acad Sci USA, **104**(32): 13005–9.
140. Stiel, A. C., S. Trowitzsch, et al. (2007). 1.8 A bright-state structure of the reversibly switchable fluorescent protein Dronpa guides the generation of fast switching variants. Biochem J, **402**(1): 35–42.
141. Wilmann, P. G., K. Turcic, et al. (2006). The 1.7 A crystal structure of Dronpa: a photoswitchable green fluorescent protein. J Mol Biol, **364**(2): 213–24.
142. Dedecker, P., J. Hotta, et al. (2006). Fast and reversible photoswitching of the fluorescent protein Dronpa as evidenced by fluorescence correlation spectroscopy. Biophys J, **91**(5): L45–7.
143. Fron, E., C. Flors, et al. (2007). Ultrafast excited-state dynamics of the photoswitchable protein Dronpa. J Am Chem Soc, **129**(16): 4870–1.
144. Mizuno, H., T. K. Mal, et al. (2008). Light-dependent regulation of structural flexibility in a photochromic fluorescent protein. Proc Natl Acad Sci USA, **105**(27): 9227–32.
145. Habuchi, S., P. Dedecker, et al. (2006). Photo-induced protonation/deprotonation in the GFP-like fluorescent protein Dronpa: mechanism responsible for the reversible photoswitching. Photochem Photobiol Sci, **5**(6): 567–76.
146. Chisari, M., D. K. Saini, et al. (2007). Shuttling of G protein subunits between the plasma membrane and intracellular membranes. J Biol Chem, **282**(33): 24092–8.
147. Wiegert, J. S., C. P. Bengtson, and H. Bading (2007). Diffusion and not active transport underlies and limits ERK1/2 synapse-to-nucleus signaling in hippocampal neurons. J Biol Chem, **282**(40): 29621–33.
148. Aramaki, S., and K. Hatta (2006). Visualizing neurons one-by-one *in vivo*: optical dissection and reconstruction of neural networks with reversible fluorescent proteins. Dev Dyn, **235**(8): 2192–9.
149. Dedecker, P., J. Hotta, et al. (2007). Subdiffraction imaging through the selective donut-mode depletion of thermally stable photoswitchable fluorophores: numerical analysis and application to the fluorescent protein Dronpa. J Am Chem Soc, **129**(51): 16132–41.
150. Betzig, E., G. H. Patterson, et al. (2006). Imaging intracellular fluorescent proteins at nanometer resolution. Science, **313**(5793): 1642–5.
151. Eggeling, C., M. Hilbert, et al. (2007). Reversible photoswitching enables single-molecule fluorescence fluctuation spectroscopy at high molecular concentration. Microsc Res Tech. 2007 DEC; **70**(12): 1003–9.
152. Egner, A., C. Geisler, et al. (2007). Fluorescence nanoscopy in whole cells by asynchronous localization of photoswitching emitters. Biophys J. NOV 1; **93**(9): 3285–90.
153. Stiel, A. C., M. Andresen, et al. (2008). Generation of monomeric reversibly switchable red fluorescent proteins for far-field fluorescence nanoscopy. Biophys J. SEP 15; **95**(6): 2989–97.
154. Campbell, R. E., O. Tour, et al. (2002). A monomeric red fluorescent protein. Proc Natl Acad Sci USA, **99**(12): 7877–82.
155. Nienhaus, G. U., K. Nienhaus, et al. (2006). Photoconvertible fluorescent protein EosFP: biophysical properties and cell biology applications. Photochem Photobiol, **82**(2): 351–8.

156. Nienhaus, K., G. U. Nienhaus, et al. (2005). Structural basis for photo-induced protein cleavage and green-to-red conversion of fluorescent protein EosFP. Proc Natl Acad Sci USA, **102**(26): 9156–9.
157. Mizuno, H., T. K. Mal, et al. (2003). Photo-induced peptide cleavage in the green-to-red conversion of a fluorescent protein. Mol Cell, **12**(4): 1051–8.
158. Shroff, H., C. G. Galbraith, et al. (2007). Dual-color superresolution imaging of genetically expressed probes within individual adhesion complexes. Proc Natl Acad Sci USA, **104**(51): 20308–13.
159. Niu, L., and J. Yu (2008). Investigating intracellular dynamics of FtsZ cytoskeleton with photo-activation single-molecule tracking. Biophys J, **95**(4): 2009–16, 15 Aug 2008.
160. Aubin, J. E. (1979). Autofluorescence of viable cultured mammalian cells. J Histochem Cytochem, **27**(1): 36–43.
161. Chance, B., and B. Thorell (1959). Localization and kinetics of reduced pyridine nucleotide in living cells by microfluorometry. J Biol Chem, **234**: 3044–50.
162. Benson, R. C., R. A. Meyer, et al. (1979). Cellular autofluorescence—is it due to flavins? J Histochem Cytochem, **27**(1): 44–8.
163. Xiao, J., J. Elf, et al. (2007). Imaging gene expression in living cells at the single-molecule level. In *Single Molecules: A Laboratory Manual*. Cold Spring Harbor Laboratory Press: Cold Spring Harbor, New York, pp. 149–69.
164. Lansford, R., G. Bearman, and S. E. Fraser (2001). Resolution of multiple green fluorescent protein color variants and dyes using two-photon microscopy and imaging spectroscopy. J Biomed Opt, **6**: 311.
165. Dickinson, M. E., G. Bearman, et al. (2001). Multi-spectral imaging and linear unmixing add a whole new dimension to laser scanning fluorescence microscopy. Biotechniques, **31**(1272): 1274–6.
166. Connally, R., D. Veal, and J. Piper (2004). Flash lamp-excited time-resolved fluorescence microscope suppresses autofluorescence in water concentrates to deliver an 11-fold increase in signal-to-noise ratio. J Biomed Opt, **9**(4): 725–34.
167. Wilkerson, C. W., Jr., P. M. Goodwin, et al. (1993). Detection and lifetime measurement of single molecules in flowing sample streams by laser-induced fluorescence. Appl Phys Lett, 62(17): 2030–32.
168. Qin, J., Y. Fung, et al. (2004). Native fluorescence detection of flavin derivatives by microchip capillary electrophoresis with laser-induced fluorescence intensified charge-coupled device detection. J Chromatogr A, **1027**(1–2): 223–29.
169. Yang, H., G. Luo, et al. (2003). *Protein Conformational Dynamics Probed by Single-Molecule Electron Transfer*. American Association for the Advancement of Science: Washington, DC: pp. 262–6.
170. Xie, X. S., J. Yu, and W. Y. Yang (2006). Living cells as test tubes. Science, **312**(5771): 228–30.
171. Straight, A. F., A. S. Belmont, et al. (1996). GFP tagging of budding yeast chromosomes reveals that protein-protein interactions can mediate sister chromatid cohesion. Curr Biol, **6**(12): 1599–1608.
172. Lau, I. F., S. R. Filipe, et al. (2003). Spatial and temporal organization of replicating *Escherichia coli* chromosomes. Mol Microbiol, **49**(3): 731–43.
173. Bertrand, E., P. Chartrand, et al. (1998). Localization of ASH1 mRNA particles in living yeast. Mol Cell, **2**(4): 437–45.
174. Averbeck, D., and S. Averbeck (1998). DNA photodamage, repair, gene induction and genotoxicity following exposures to 254 nm UV and 8-methoxypsoralen plus UVA in a eukaryotic cell system. Photochem Photobiol, **68**(3): 289–95.
175. Pfeifer, G. P., R. Drouin, et al. (1992). Binding of transcription factors creates hot spots for UV photoproducts *in vivo.* Mol Cell Biol, **12**(4): 1798.
176. Jones, C. A., E. Huberman, et al. (1987). Mutagenesis and cytotoxicity in human epithelial cells by far-and near-ultraviolet radiations: action spectra. Radiat Res, **110**(2): 244–54.
177. Mohanty, S. K., M. Sharma, and P. K. Gupta (2006). Generation of ROS in cells on exposure to CW and pulsed near-infrared laser tweezers. Photochem Photobiol Sci, **5**(1): 134–9.
178. Neuman, K. C., E. H. Chadd, et al. (1999). Characterization of photodamage to *Escherichia coli* in optical traps. Biophys J, **77**(5): 2856–63.
179. Liu, Y., G. J. Sonek, et al. (1996). Physiological monitoring of optically trapped cells: assessing the effects of confinement by 1064-nm laser tweezers using microfluorometry. Biophys J, **71**(4): 2158.
180. Ashkin, A., and J. M. Dziedzic (1989). Internal cell manipulation using infrared laser traps. Proc Natl Acad Sci USA, **86**(20): 7914–18.
181. Moan, J., K. Berg, et al. (1989). Intracellular localization of photosensitizers. In *Photosensitizing Compounds: Their Chemistry, Biology and Clinical Use*, G. Bock and S. Harnett, Editors. John Wiley and Sons: New York, pp. 95–111.

182. Bensasson, R. V., E. J. Land, and T. G. Truscott (1993). *Excited States and Free Radicals in Biology and Medicine*. Oxford University Press: Oxford.
183. Dixit, R., and R. Cyr (2003). Cell damage and reactive oxygen species production induced by fluorescence microscopy: effect on mitosis and guidelines for non-invasive fluorescence microscopy. Plant J, **36**(2): 280–90.
184. Halliwell, B., and J. M. C. Gutteridge (1989). Protection against oxidants in biological systems: the superoxide theory of oxygen toxicity. Free Rad Biol Med. Edited by Halliwell B, Gutteridge JMC, Oxford Clarendun Press pp 86–179.
185. Schafer, F. Q., and G. R. Buettner (2001). Redox environment of the cell as viewed through the redox state of the glutathione disulfide/glutathione couple. Free Rad Biol Med, **30**(11): 1191–1212.
186. de With, A., and K. O. Greulich (1995). Wavelength dependence of laser-induced DNA damage in lymphocytes observed by single-cell gel electrophoresis. J Photochem Photobiol B Biol, **30**(1): 71–76.
187. Tripathi, A., R. E. Jabbour, et al. (2008). Waterborne pathogen detection using Raman spectroscopy. Appl Spectrosc, **62**: 1–9.
188. Benson, D. M., J. Bryan, et al. (1985). Digital imaging fluorescence microscopy: spatial heterogeneity of photobleaching rate constants in individual cells. J Cell Biol, **100**(4): 1309–23.
189. Adachi, K., K. Kinosita, Jr., and T. Ando (1999). Single-fluorophore imaging with an unmodified epifluorescence microscope and conventional video camera. J Microsc, **195**(2): 125–32.
190. Gratton, E., and M. J. vandeVen (1995). *Laser sources for confocal microscopy*, in *Handbook of Biological Confocal Microscopy*, J. B. Pawley, Editor. Plenum Press: New York, pp. 65–98.
191. Murphy, D. B. (2002). *Fundamentals of Light Microscopy and Electronic Imaging*. Wiley-Liss: New York.
192. Nipkow, P. (1884). German Patent 30,105.
193. Inoue, S., and K. R. Spring (1997). *Video Microscopy*. Plenum Press: New York.
194. Stuurman, N., and R. D. Vale (2006). Imaging single molecules using total internal reflection fluorescence microscopy. In *Live Cell Imaging, A Laboratory Manual*, R.D. Goldman and D.L. Spector, Editors. Cold Spring Harbor Laboratory Press: Cold Spring Harbor, New York, pp. 585–601.
195. Swedlow, J. R., P. D. Andrews, and M. Platani (2005). *In vivo* imaging of mammalian cells. In *Live Cell Imaging: A Laboratory Manual*. Cold Spring Harbor Laboratory Press: Cold Spring Harbor, New York, pp. 329–43.
196. Elf, J., G. W. Li, and X. S. Xie (2007). Probing transcription factor dynamics at the single-molecule level in a living cell. Science, **316**(5828): 1191–4.
197. Ueda, M., Y. Sako, et al. (2001). Single-molecule analysis of chemotactic signaling in *Dictyostelium* cells. Science, **294**(5543): 864–7.
198. Haggie, P. M., and A. S. Verkman (2008). Monomeric CFTR in plasma membranes in live cells revealed by single-molecule fluorescence imaging. J Biol Chem. AUG 2008; **283**: 23510–23513.
199. Fu, G., C. Wang, et al. (2008). Heterodimerization of integrin Mac-1 subunits studied by single-molecule imaging. Biochem Biophys Res Commun, **368**(4): 882–6.
200. Ulbrich, M. H., and E. Y. Isacoff (2007). Subunit counting in membrane-bound proteins. Nat Methods, **4**(4): 319–21.
201. Groc, L., M. Heine, et al. (2004). Differential activity-dependent regulation of the lateral mobilities of AMPA and NMDA receptors. Nat Neurosci, **7**(7): 695–6.
202. Lommerse, P. H., G. A. Blab, et al. (2004). Single-molecule imaging of the H-ras membrane-anchor reveals domains in the cytoplasmic leaflet of the cell membrane. Biophys J, **86**(1 Pt 1): 609–16.
203. Lommerse, P. H., B. E. Snaar-Jagalska, et al. (2005). Single-molecule diffusion measurements of H-Ras at the plasma membrane of live cells reveal microdomain localization upon activation. J Cell Sci, **118**(Pt 9): 1799–809.
204. Sonnleitner, A., L. M. Mannuzzu, et al. (2002). Structural rearrangements in single ion channels detected optically in living cells. Proc Natl Acad Sci USA, **99**(20): 12759.
205. Cai, D., K. J. Verhey, and E. Meyhofer (2007). Tracking single Kinesin molecules in the cytoplasm of mammalian cells. Biophys J, **92**(12): 4137–44.
206. Holland, M. J. (2002). Transcript abundance in yeast varies over six orders of magnitude. J Biol Chem, **277**(17): 14363–6.
207. Velculescu, V. E., L. Zhang, et al. (1997). Characterization of the yeast transcriptome. Cell, **88**(2): 243–51.
208. Novick, A., and M. Weiner (1957). Enzyme induction as an all-or-none phenomenon. Proc Natl Acad Sci USA, **43**(7): 553–66.
209. Blake, W. J., M. Kærn, et al. (2003). Noise in eukaryotic gene expression. Nature, **422**(6932): 633–7.
210. Raser, J.M., and E. K. O'Shea (2004). Control of stochasticity in eukaryotic gene expression. Science, **304**(5678): 1811–4.

211. Kohout, S. C., M. H. Ulbrich, et al. (2008). Subunit organization and functional transitions in Ci-VSP. Nat Struct Mol Biol, **15**(1): 106–8.
212. Joglekar, A. P., D. C. Bouck, et al. (2006). Molecular architecture of a kinetochore-microtubule attachment site. Nat Cell Biol, **8**(6): 581–5.
213. Hess, S. T., T. J. Gould, et al. (2007). Dynamic clustered distribution of hemagglutinin resolved at 40 nm in living cell membranes discriminates between raft theories. Proc Natl Acad Sci USA, **104**(44): 17370–5.
214. Patterson, G. H., et al. (1997). Use of the green fluorescent protein and its mutants in quantitative fluorescence microscopy. Biophys J, **73**(5): 2782–90.
215. Iwane, A. H., et al. (1997). Single molecular assay of individual ATP turnover by a myosin-GFP fusion protein expressed *in vitro*. FEBS Lett, **407**(2): 235–8.
216. Cognet, L., et al. (2002). Fluorescence microscopy of single autofluorescent proteins for cellular biology. C R Physique, **3**(5): 645–56.
217. Kremers, G. J., et al. (2007). Improved green and blue fluorescent proteins for expression in bacteria and mammalian cells. Biochemistry, **46**(12): 3775–83.
218. Hendrix, J., et al. (2008). Dark states in monomeric red fluorescent proteins studied by fluorescence correlation and single molecule spectroscopy. Biophys J, **94**(10): 4103.